The influence of synorogenic extension on the crustal architecture of North Gondwana during the assembly of Pangaea (Ossa–Morena Zone, SW Iberia)

Ícaro Dias da Silva[1]*, Manuel Francisco Pereira[2], Cristina Gama[2], Lourenço Steel Hart[1], Santos Barrios Sánchez[3], Kelvin dos Santos Alves[3], Juan Gómez Barreiro[3], Colombo Celso Gaeta Tassinari[4] and Kei Sato[4]

[1]Faculdade de Ciências, Instituto Dom Luiz, Universidade de Lisboa, Campo Grande, Edifício C1, Piso 1, 1749-016 Lisboa, Portugal

[2]Departamento de Geociências, Instituto de Ciências da Terra, Universidade de Évora, Apt. 94, 7002-554 Évora, Portugal

[3]Departamento de Geología, Universidad de Salamanca, Plaza de la Merced, s/n, 37008 Salamanca, Spain

[4]Instituto de Energia e Ambiente/Instituto de Geociencias, Universidade de São Paulo, Av. Luciano Gualberto, 1289, Cidade Universitária, 05508-010 São Paulo, Brazil

IDS, 0000-0002-0185-9410; MFP, 0000-0001-9032-2318
*Correspondence: ifsilva@ciencias.ulisboa.pt

Abstract: We present a new structural study of a D_2–M_2 tectono-thermal structure in SW Iberia (Ponte de Sor–Seda gneiss dome) characterized by a spatial distribution of telescoping isograds providing a record of Buchan-type metamorphic conditions. The gneiss dome comprises an infrastructure made up of a lower gneiss unit (LGU) and an intermediate schist unit (ISU), separated by early D_2 ductile extensional shear zones. The LGU and the ISU are composed of Ediacaran–Cambrian rocks that experienced the highest-grade M_2 metamorphic conditions (amphibolite facies). Late Ediacaran–Early Terreneuvian and Late Miaolingian–Early Furongian protolith ages for LGU (496 ± 3 Ma) and ISU (539 ± 2 Ma) orthogneisses are reported. A superstructure made of Cambrian–Devonian rocks (Upper Slate Unit, USU) deformed under M_2 greenschist facies conditions, tectonically overlies the ISU across a D_2 extensional shear zone. Kinematic criteria associated with D_2–M_2 fabrics indicate top-to-ESE–SE sense of shear. A late-D_2 brittle-ductile high-angle extensional shear zone (Seda shear zone) crosscuts the gneiss dome. D_3 upright folds, thrusts and transpressive shear zones caused the steepening of D_2 structures and the local crenulation of S_2 foliation. The Mississippian D_2–M_2 event recorded in the Ossa–Morena Zone may be regarded as a regional-scale phenomenon that markedly influenced the crustal architecture of North Gondwana during the assembly of Pangaea.

Supplementary material: Thin section and geochronology sample location and U-Pb data table of SHRIMP analysis of zircon grains (samples CHA-2.1 and VAL-4.1) are available at https://doi.org/10.6084/m9.figshare.c.6828875

Partial melting of the continental crust has a profound impact on orogenic evolution as it causes weakening of the orogenic root and favours gravity-driven lateral flow and/or the development of gravitational instabilities (Vanderhaeghe 2009). Partial melting occurs as a result of tectonic crustal thickening involving terranes with high radioactive heat production and under specific kinematic regimes (Collins 2002; Vanderhaeghe 2012). The formation of tectono-thermal structures typically composed of a core of gneisses and migmatites, structurally overlain by metamorphic rocks of much lower metamorphic grade, can be classified as gneiss domes (Teyssier and Whitney 2002; Whitney *et al.* 2004; Yin 2004) or metamorphic core complexes (Coney 1980; Dewey 1988). The exchange of arguments on the classification of dome-like tectono-thermal structures, including consideration of the relationship between metamorphic core complexes and gneiss domes, is useful for a better understanding of the extensional exhumation processes (e.g. Whitney *et al.* 2013; Platt *et al.* 2015), but is beyond the scope of this study. Some metamorphic core complexes may include gneiss domes in their lower unit (e.g. Vanderhaeghe *et al.* 1999*a*; Vanderhaeghe 2004) complicating structure definition. Dome structures are flanked by flat-lying ductile extensional shear zones developed at mid-lower crustal levels along with migmatites and gneisses, which are exhumed and juxtaposed with upper crustal units

From: Nance, R. D., Strachan, R. A., Quesada, C. and Lin, S. (eds) 2024. *Supercontinents, Orogenesis and Magmatism*. Geological Society, London, Special Publications, **542**, 549–578.
First published online November 3, 2023, https://doi.org/10.1144/SP542-2023-9

(Vanderhaeghe *et al.* 1999*b*). The upper crust is deformed by brittle extensional faulting, forming an array of extensional horst-and-graben systems, coexisting with synorogenic sedimentation and volcanism (Wernicke 1981).

In this study, we review the geology of a region of SW Iberia included in the European Variscan orogenic belt, formed within the Gondwana–Laurussia convergent margin during the Late Paleozoic assembly of the supercontinent Pangaea (Matte 2001; Murphy and Nance 2013). This is an exceptionally good natural laboratory for describing such tectono-thermal structures (Vanderhaeghe *et al.* 2020; Schulmann *et al.* 2022). At the westernmost tip of the Variscan belt, similar gneiss domes are exposed in the continental basement of Iberia (Fig. 1a), representing the North Gondwana continental margin. Mississippian gneiss domes are found in NW Iberia (Escuder Viruete *et al.* 1994; Díez Balda *et al.* 1995; Díez Fernández and Pereira 2016; Dias da Silva *et al.* 2017, 2021) and SW Iberia (Apraiz and Eguíluz 2002; Pereira *et al.* 2009; Dias da Silva *et al.* 2018). These partially molten rocks have been interpreted as being a key variable in determining the rate of crustal flow during orogenic gravitational collapse. In NW Iberia, gneiss domes are considered to be intimately linked to extensional structures (Escuder Viruete *et al.* 1994; Díez Balda *et al.* 1995; Díez Fernández *et al.* 2012, 2017; Díez Fernández and Pereira 2016; Dias da Silva *et al.* 2021). After the tectonic formation of the Variscan allochthonous wedge, gneiss domes may have been generated by regional extension that caused the flow of partially molten crust at depth and the exhumation of high-temperature and low-pressure metamorphic rocks. In SW Iberia, the Variscan gneiss domes show similar features to those of NW Iberia, while arc-like mafic-intermediate igneous rocks are dominant in the former (Rodríguez *et al.* 2022). As an alternative to the tectonic model put forward for NW Iberia, the underlying mechanism for explaining the ongoing long-term extension causing the exhumation of migmatite–granite in SW Iberia was the rollback of the subducting slab (i.e. Paleotethys Ocean) beneath the North Gondwana margin (Pereira *et al.* 2022*a*, *b*). Another model for the tectonic evolution of SW Iberia suggests that a mantle plume was emplaced during the Mississippian beneath the North Gondwana continental crust, and heat released from the plume led to melting of the overlying crust, explaining the voluminous granitic magmatism and associated mantle-derived mafic magmas (i.e. Iberian Reflective Body; Simancas *et al.* 2003). Although there are several models being debated for the evolution of the Variscan orogen in Iberia, questions still prevail regarding how the crustal architecture of SW Iberia evolved during the Carboniferous.

The aim of this paper is to present original structural, petrological and geochronological data on the poorly known Ponte de Sor–Seda region representing a Variscan tectono-thermal structure exposed in SW Iberia, referred to as a gneiss dome. The new findings make it possible to discuss the tectonic evolution of the Variscan orogenic belt, taking the Ossa–Morena Zone (OMZ) as the key Paleozoic tectonic unit of SW Iberia (Fig. 1b), by assuming that partial melting of the thickened crust may have caused weakening of the lower crustal levels, leading to gravity-driven lateral flow and/or the development of gravitational instabilities during the Mississippian. In addition, new crystallization ages for the Valongo and Chancelaria orthogneisses are used to update the Geological Map of Portugal (scale 1:50 000; Galopim de Carvalho *et al.* 1981) and provide a better understanding of the temporal scope of the magmatic activity in the OMZ as part of the North Gondwana margin during the Cambrian.

Geological framework

The diachronic collision between Gondwana and Laurussia started in the Middle–Upper Devonian, associated with the closure of the Rheic Ocean, and ended with the formation of the Variscan belt in Iberia (Matte 2001; Martínez Catalán *et al.* 2009). The structure of SW Iberia is complex, resulting from the interaction of successive contractional and extensional deformation events associated with the development of the Variscan orogeny. It shows similarities with that of NW Iberia (Díez Fernández and Arenas 2015; Díez Fernández *et al.* 2016). To determine the structure of SW Iberia, we first summarize what is known about that of NW Iberia, which better preserves the early deformation and metamorphism events (D_1–M_1) of the Variscan orogeny.

The transition from an accretionary to collisional orogen in NW Iberia is marked by the tectonic emplacement and unrooting of an accretionary wedge along the North Gondwana margin (Arenas *et al.* 1986; Gómez Barreiro *et al.* 2007; Martínez Catalán *et al.* 2009). In accordance with this tectonic model, North Gondwana represents the lower plate that was partially subducted in the Famennian after the subduction of the Rheic oceanic lithosphere, while Laurussia acted as the upper plate (Arenas *et al.* 2014). This rootless Variscan accretionary wedge includes a basal allochthonous unit (Abati *et al.* 2010; Díez Fernández *et al.* 2010) representing tectonic slices of subducted continental crust that experienced high-pressure metamorphism at *c.* 370–363 Ma (Rodríguez *et al.* 2003; López-Carmona *et al.* 2014). Later, it was tectonically emplaced onto the North Gondwana autochthon (i.e. Central Iberian Zone, CIZ) (Martínez Catalán

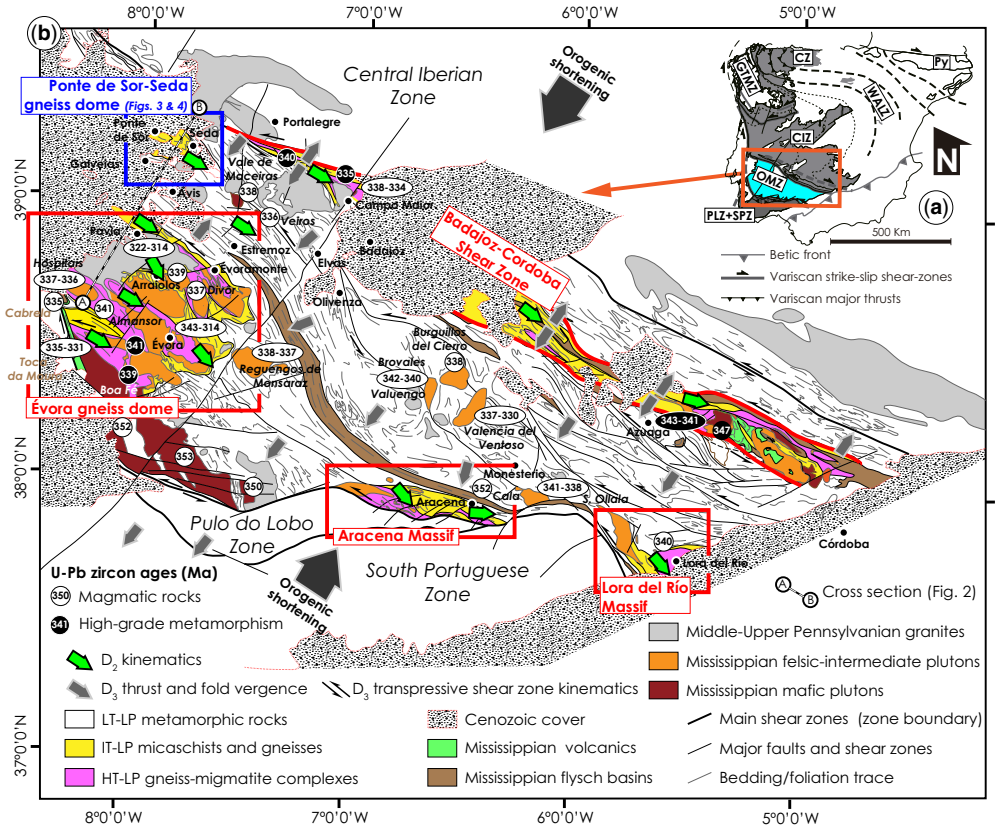

Fig. 1. (**a**) Sketch map of the Iberian Massif: OMZ, Ossa–Morena Zone; CIZ, Central Iberian Zone; CZ, Cantabrian Zone; GTMZ, Galicia–Trás-os-Montes Zone; PLZ, Pulo do Lobo Zone; SPZ, South Portuguese Zone; WALZ, West Asturian Leonese Zone. (**b**) Schematic geological map of the OMZ showing the location of the Ponte de Sor–Seda gneiss dome in relation to the Évora gneiss dome, the Aracena and Lora del Río massifs, and the Badajoz–Córdoba Shear Zone (based on 1:50.000 and 1:200.000 scale geological maps of Portugal, LNEG, and Spain, IGME-CSIC). The numbers refer to the age in millions of years of plutonism (circles and ellipses in white) and of high grade-metamorphic rocks (circles and ellipses in black). Note that the tectonic transport direction towards the ESE–SE related to the D_2 extensional event (this study) does not coincide with the vergence towards the SW of the thrusts and folds (Matte 2007), the orogenic polarity (Franke 2000) or the collisional transport direction towards the SW (Rubio Pascual *et al.* 2016) in Pennsylvanian times (i.e. D_3 contractional event). Source: (a) simplified from Martínez Catalán (2011). (b) The geochronological data are compiled from Montero *et al.* (2000), Romeo *et al.* (2006), Pin *et al.* (2008), Azor *et al.* (2008), Pereira *et al.* (2009, 2012*a*, 2015, 2020*a*, 2023*a*), Antunes *et al.* (2011), Lima *et al.* (2012), Moita *et al.* (2015), Cambeses *et al.* (2015), Dias da Silva *et al.* (2018) and Rodríguez *et al.* (2022).

et al. 2009). There is also a parautochthonous unit that represents an imbricated thrust and fold sequence lying atop a basal shear zone, defining the boundary with the underlying autochthon (Dias da Silva *et al.* 2021).

In NW Iberia, the tectonic emplacement of the allochthonous units at *c.* 360–340 Ma caused initial Variscan folds and later thrusts recognized in the parautochthon and in the CIZ autochthon (D_1–M_1, as defined by Dias da Silva *et al.* 2021 and references therein). Physical conditions for the regional Mississippian synorogenic collapse in the region and the rebound of the underlying autochthon (i.e. CIZ) were triggered by the tectonic overburden. The tectonic instability that prevailed in at this stage of orogenic evolution favoured the formation of large-scale D_2–M_2 gneiss domes at *c.* 340–320 Ma (Gutiérrez-Alonso *et al.* 2018; López-Moro *et al.* 2018; Rubio Pascual *et al.* 2022; Martins *et al.* 2021). The development of these D_2–M_2 extensional macro-structures overprinted previous fabrics and the allochthonous thrust sheet (Díez Fernández *et al.* 2012). A Pennsylvanian D_3 contractional deformation event is recognized in the gneiss

domes (Díez Fernández and Pereira 2016) and the synorogenic basins of NW Iberia (González Clavijo *et al.* 2021), through having caused NW–SE upright folding and through the formation of transcurrent conjugate shear zones.

In SW Iberia, the OMZ, composed of Ediacaran to Pennsylvanian rocks, represents the continental margin of North Gondwana (Martínez Catalán *et al.* 2007). At its southern extremity, it is in contact across Variscan transpressive faults (Simancas *et al.* 2009) with the Devonian and Carboniferous rocks of the Pulo do Lobo (PLZ) and South Portuguese zones (SPZ), which are part of the Laurussia margin (Pereira *et al.* 2017) (Fig. 1b).

The OMZ stratigraphy is composed of Ediacaran to Upper Carboniferous sedimentary sequences and volcanic rocks associated with pre- and syn-Variscan stages of the geodynamic evolution (Quesada 1996) that includes: (i) the onset of a Late Ediacaran Cadomian magmatic arc and synorogenic sedimentation (Eguíluz *et al.* 2000; Linnemann *et al.* 2008) and transition to a Cambrian–Ordovician magma-rich rifted continental margin (Sánchez-García *et al.* 2003), followed by (ii) Upper Ordovician–Lower Devonian passive margin sedimentation associated with the opening of the Paleozoic Rheic Ocean (Gutiérrez-Marco and Robardet 2004) and (iii) Carboniferous Variscan synorogenic sedimentation (Pereira *et al.* 2020*b*) and an arc-type magmatic flare-up (Pereira *et al.* 2022*b*) during the assembly of the Pangaea supercontinent.

In SW Iberia, there are a few occurrences of high-pressure metamorphic rocks which formed at *c.* 377–371 Ma (Moita *et al.* 2005; Abati *et al.* 2018) and which predate the main foliation of the OMZ, but these are less well represented than in NW Iberia. Variable-size boudins of eclogites and blueschist are surrounded by a pervasive Mississippian mylonitic foliation developed in marbles and quartzofeldspathic gneisses (Pereira *et al.* 2007, 2012*a*). In SW Iberia, structures related to the early Variscan deformation and metamorphic events (D_1–M_1) are quite difficult to find because they are generally overprinted by a Mississippian foliation associated with the second Variscan deformation and metamorphism event (D_2–M_2). This Mississippian deformation event led to retrograde metamorphism of D_1–M_1 high-*P*–intermediate-high-*T* mineral assemblages and fabrics as a response to rapid decrease in pressure associated with the development of the S_2 foliation (Pereira *et al.* 2010; Abati *et al.* 2018; Arenas *et al.* 2021; Novo-Fernández *et al.* 2021). The Cambrian–Silurian OMZ metasedimentary rocks were deformed into recumbent folds and later overlaid by Upper Devonian–Mississippian sedimentary rocks (Quesada *et al.* 1990). These recumbent folds have been assigned to the first Variscan contractional deformation event (Simancas *et al.* 2001) but this interpretation has been challenged with the use of new geochronological data and a new tectonic model, the authors of which argue that the recumbent folds and the main foliation of the OMZ were formed during Mississippian intra-orogenic D_2–M_2 extension (Pereira *et al.* 2023*a*). A third Variscan deformation and metamorphism event (D_3–M_3), overlapping, S_2 foliation, led to the development of upright folds, an S_3 crenulation cleavage and transpressive shear zones (Dias da Silva *et al.* 2018). The structure resulting from D_3–M_3 produced the outcrop pattern of the pre-Mesozoic rocks of the OMZ (Pereira *et al.* 2009, 2023*b*; Dias da Silva *et al.* 2018; Díez Fernández *et al.* 2021), before Alpine deformation (Fig. 2).

The spatial distribution of the Variscan structures and D_2–M_2 fabrics in the OMZ is extremely heterogeneous. In some areas under the influence of the Variscan gneiss domes, D_2 is so marked that it erases previous sedimentary and tectonic structures. In contrast, in other areas not far from Variscan gneiss domes, D_2 is either absent or so weak that the original Ediacaran–Lower Devonian stratigraphy (sedimentary structures and unconformities) and previous Cadomian structures (foliation, stretching lineation and folds) can be recognized, having been barely touched by Variscan deformation.

The regional distribution of M_2 Buchan-type (low-pressure–high-temperature) isograds, S_2 foliation, Le_2 stretching lineation, shear zones and folds has enabled the recognition of kilometre-scale Mississippian gneiss domes in the OMZ (Fig. 1b): (i) the Lora del Río-Aracena–Évora metamorphic belt (Pereira *et al.* 2009; Dias da Silva *et al.* 2018) located near the boundary with the PLZ and the SPZ, and (ii) the Badajoz–Cordoba shear zone (Quesada and Dallmeyer 1994) or Central Unit (Azor *et al.* 1994), located close to the boundary with the CIZ, which has recently been reinterpreted as a Variscan gneiss dome later deformed by D_3 transpressive shear zones and folding (Pereira *et al.* 2023*a*).

In the OMZ, Variscan gneiss domes share tectono-metamorphic features and show many similarities with the architectural model organized on the general concepts of 'infrastructure' and 'superstructure' that were first applied to the Late Paleozoic gneiss domes of the Pyrenees by Zwart (1979) and later revisited by Denèle *et al.* (2007) and Vanardois *et al.* (2022). Therefore, it is assumed that the infrastructure of the OMZ gneiss domes is generally composed, from bottom to top (Fig. 2) of: (i) a migmatite-gneiss unit (MGU), (ii) a lower gneiss unit (LGU) and (iii) an intermediate schist unit (ISU), as described by Dias da Silva *et al.* (2018) for the Évora gneiss dome, and by Dias da Silva *et al.* (2021) for NW Iberia. Another important feature is that the infrastructure, considered to be dominated by originally flat-lying structures, was the host

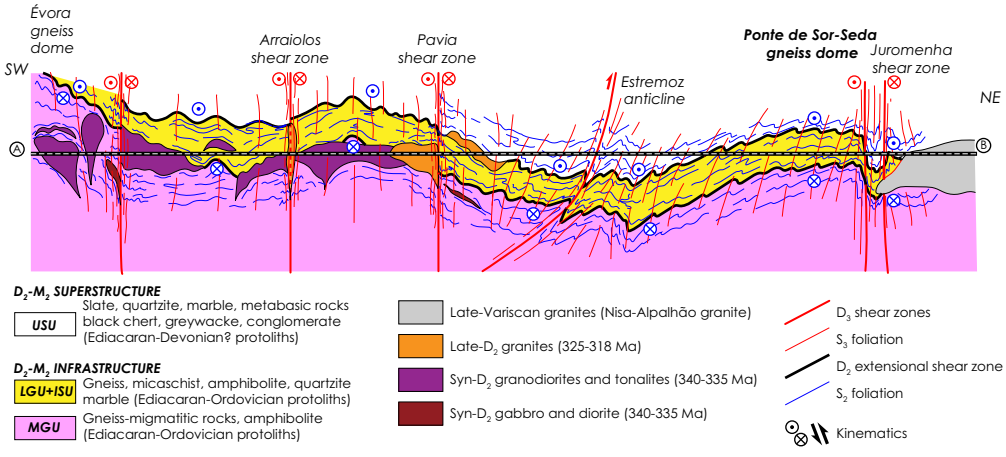

Fig. 2. Schematic geological section across the OMZ (the location of the cross-section A–B is shown in Fig. 1b) showing the Variscan crustal architecture formed by the interplay between D_2 gneiss domes and D_3 contractional structures.

for granitic and gabbro-dioritic rocks dated at *c.* 340–335 Ma (Moita *et al.* 2015; Pereira *et al.* 2015, 2022*b*, 2023*b*; Dias da Silva *et al.* 2018; Rodríguez *et al.* 2022). These contrasting tectono-metamorphic units (MGU, LGU and ISU), showing a pervasive mylonitic fabric, are separated by formerly flat-lying D_2 extensional shear zones that mimic telescoped M_2 isograds (Pereira *et al.* 2009, 2023*a*; Dias da Silva *et al.* 2018).

The gneiss dome superstructure is defined by the upper slate unit (USU; Dias da Silva *et al.* 2018). The USU is tectonically underlain by an early D_2 extensional shear zone that separates it from the infrastructure. Locally, late-D_2 brittle-ductile high-angle extensional shear zones crosscut the dome structure, enhancing the metamorphic difference between the dome core and its hanging wall, as is recognized in the Lora del Río Massif (Apraiz and Eguíluz 2002). Field relationships between Visean to Bashkirian igneous intrusions and the main foliation of the Variscan gneiss dome provide a maximum and a minimum age for D_2–M_2, respectively.

Mississippian synorogenic sedimentary basins displaying significant volcanism are described in the Superstructure (Fig. 1b), sometimes in the vicinity of Variscan gneiss domes, as is the case in the Cabrela marine basin (Pereira *et al.* 2020*b*). The development of these synorogenic basins is closely associated with the infrastructure dynamics as they are usually detached and deformed by D_2 at their contact with the underlying metamorphic basement rocks.

Brittle-ductile D_3 transpressive shear zones, thrusts and upright folds are superimposed on the S_2 foliation (Pereira *et al.* 2009, 2023*b*; Dias da Silva *et al.* 2018). As a result of this superposition, the S_2 foliation becomes steeper and may be transposed by the S_3 crenulation cleavage (Fig. 2) formed under low-grade to very-low-grade metamorphic conditions.

The Ponte de Sor–Seda gneiss dome: geometry, kinematics and tectono-thermal evolution

The Ponte de Sor–Seda gneiss dome (PSGD) occupies 200 km^2 in the central-western OMZ as part of the Barrancos–Hinojales domain (Apalategui *et al.* 1990), between the Évora gneiss dome and the Badajoz–Cordoba shear zone (Figs 1b and 2). The PSGD is partially covered by Cenozoic sedimentary rocks of the Tagus River basin and is bounded by NNE–SSW to ESE–WNW-trending steeply dipping Alpine brittle faults (Figs 3 and 4). Like the nearby Variscan gneiss domes (Évora gneiss dome and Badajoz–Cordoba shear zone; Pereira *et al.* 2023*a*), it presents a general structure dominated by pervasive S_2 foliation, heterogeneously transposed by open upright D_3 folds with fold axes variably plunging towards the NW or SE, which may be locally reoriented by NW–SE-trending brittle-ductile D_3 transpressive shear zones (Figs 3–5).

New data on field relationships and microdeformation enable the Geological Map of Portugal (Galopim de Carvalho *et al.* 1981) to be updated, by reinterpreting the tectono-metamorphic architecture of the region between Ponte de Sor and Seda, within the structural framework of a gneiss dome (Figs 2–5). The regional distribution and general characteristics of the fabrics of the PSGD allow two successive Variscan deformation–metamorphic events (D_2 extension and M_2 high-to-low-grade

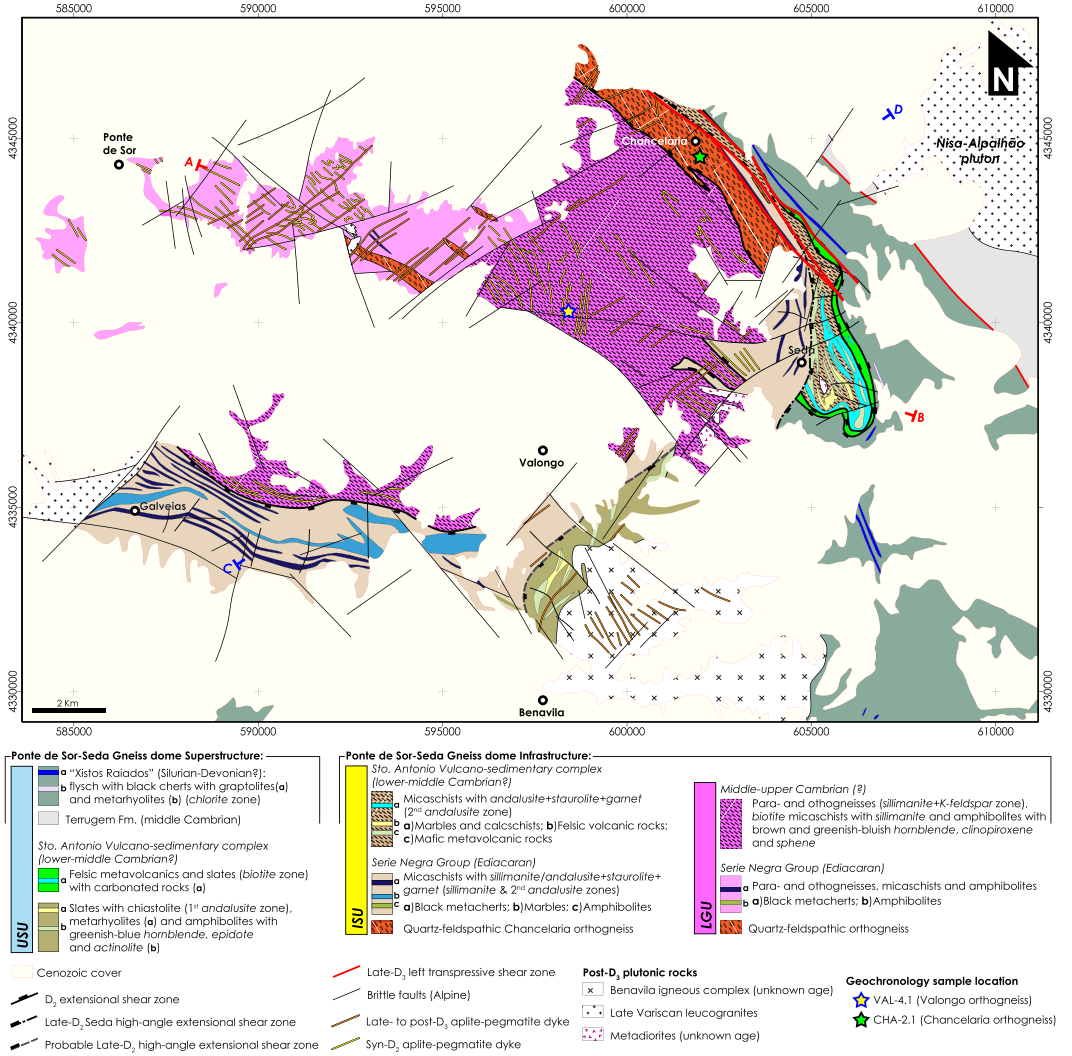

Fig. 3. Geological map of the Ponte de Sor–Seda gneiss dome showing the lithological associations of each tectono-metamorphic unit of the infrastructure (LGU, lower gneiss unit; ISU, intermediate slate unit) and the superstructure (USU, upper slate unit). This new map is a revision of the Geological Map of Portugal. Source: Galopim de Carvalho *et al.* (1981).

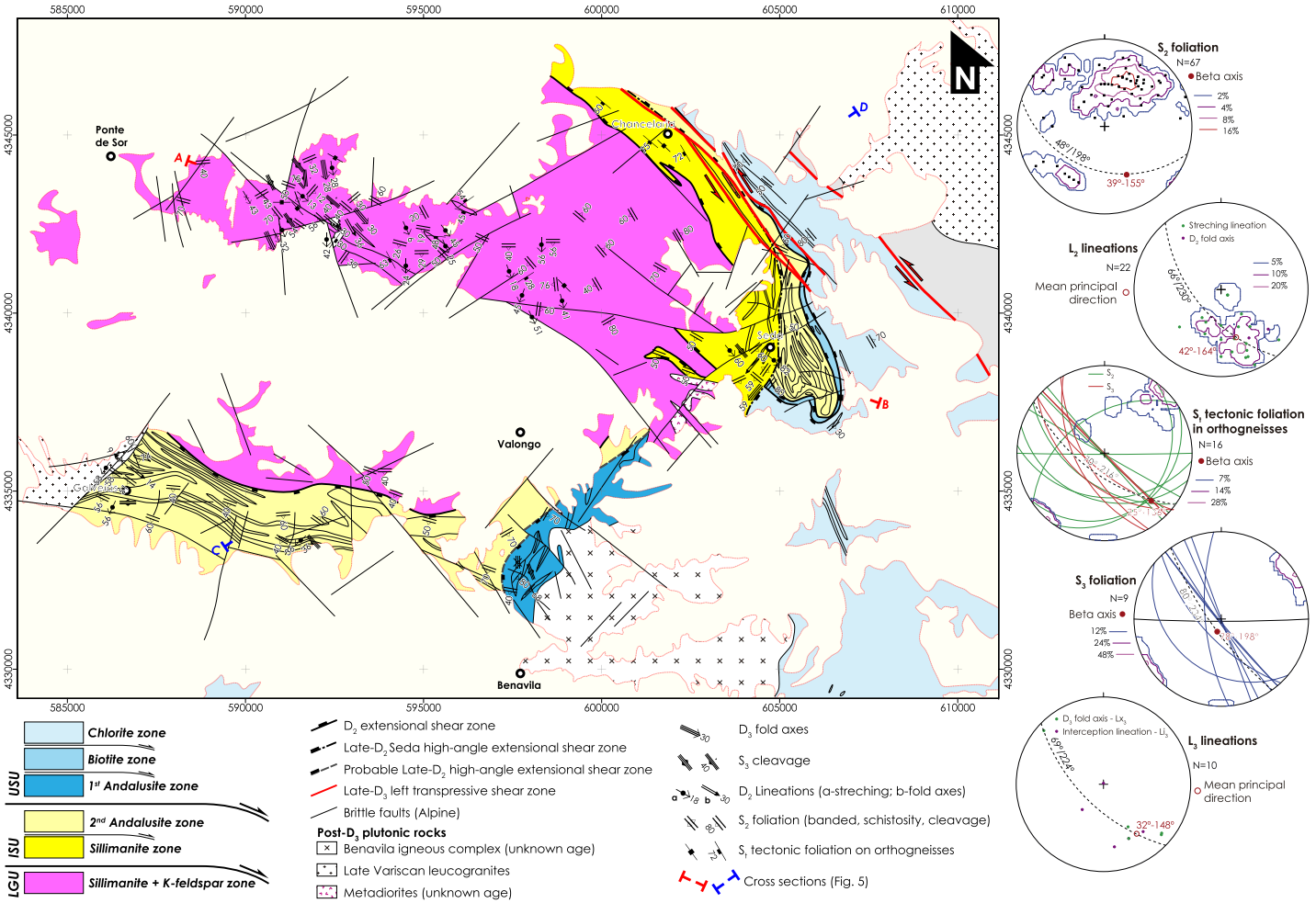

Fig. 4. Structural and metamorphic map of the Ponte de Sor–Seda gneiss dome. Equal area, lower hemisphere stereoplots showing the orientation of the S_2 foliation, L_2 (stretching lineation and fold axes), S_3 foliation and L_3 lineation.

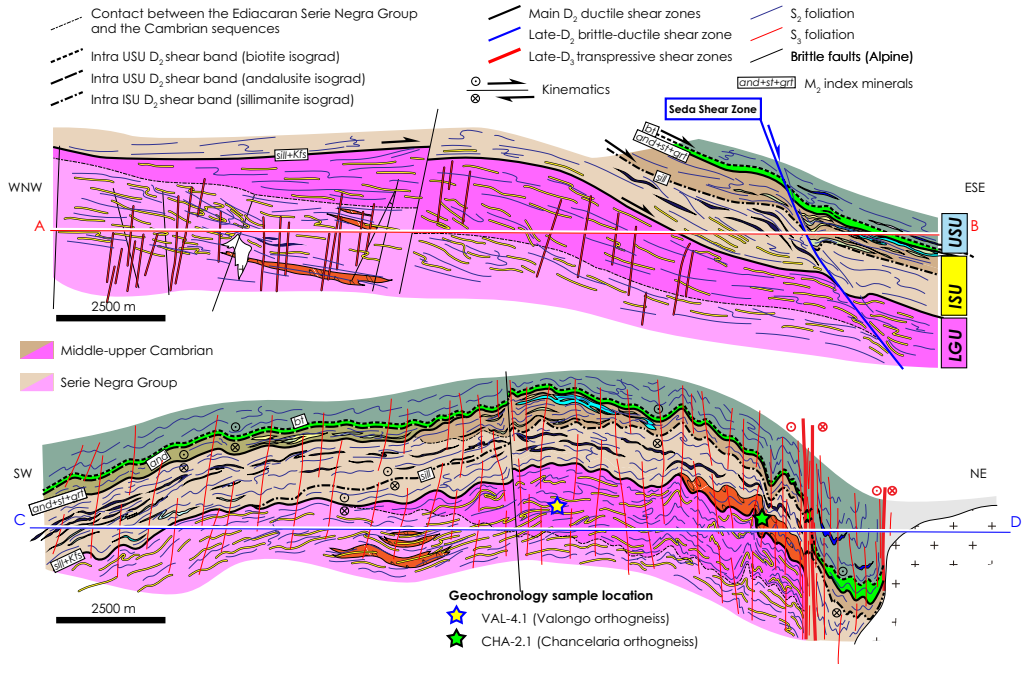

Fig. 5. Cross-sections of the Ponte de Sor–Seda gneiss dome. The location of the cross-sections A–B (WNW–ESE-trending) and C–D (SW–NE-trending) are shown in Figures 3 and 4. Infrastructure LGU and ISU and superstructure USU.

metamorphism and D_3 contraction and M_3 low-grade metamorphism) to be recognized, as previously described for the nearby Évora gneiss dome (Pereira *et al.* 2009; Dias da Silva *et al.* 2018). D_1–M_1, related to an earlier episode of crustal thickening, is poorly preserved in this sector of the OMZ. S_1 foliation was most likely transposed by D_2 ductile deformation in all tectono-metamorphic units of the PSGD. S_1 is rarely recognized in microlithons (or microfold hinges) of minor tight D_2 isoclinal folds, or as inclusion trails in syn-D_2 porphyroblasts.

D_2 is associated with two foliations formed during non-coaxial progressive deformation. S_{2a} foliation is progressively folded, developing very tight to isoclinal folds whose axial plane foliation is considered S_{2b} foliation. The PSGD is divided by an early D_2–M_2 detachment into two structural domains: the infrastructure and the superstructure. The infrastructure includes two main tectono-stratigraphic units separated by an early D_2 extensional shear zone: the LGU and the ISU. The MGU is not currently exposed in this region, contrary to the case in the Évora gneiss dome. The superstructure is represented by the upper slate unit (USU), which is composed of lower-grade metamorphic rocks, mantling the higher-temperature metamorphic core. Across the gneiss dome, a progressive change in M_2 metamorphism is observed, with a sharp increase in metamorphic grade towards the west, from Seda to Ponte de Sor (Figs 3–5).

In the PSGD, the main foliation S_2 is pervasive in all tectono-metamorphic units and commonly associated with pervasive mylonitization, transposing bedding and foliation S_1. The average dip–dip direction of S_2 foliation is 48°/198° with a beta axis of 39°–155°, which is close to the average direction of the D_3–M_3 intersection lineation and fold axes (Lx_3 and Li_3; Fig. 4). S_2 mylonitic foliation anastomoses and is folded by progressive deformation on a large variety of scales, including intrafolial folds. The S_2 foliation dip varies and is found to be vertical and parallel to the S_3 foliation due to D_3 folding (Fig. 5). D_2 ductile kinematic indicators with respect to fabric symmetry (i.e. sigmoid-shaped mineral grains, S–C foliation pairing and synthetic C' shear bands) are common and indicate a general top-to-the-SE–ESE sense of shear (Fig. 5). Recognized disharmonic intrafolial folds and conjugate shear bands (with top-to-the-NW and to-the-SE sense of shear) indicate that vertical shortening occurred locally. These late structures are the result of pure shearing in a dominant simple shear deformation regime with general NW–SE-trending horizontal stretching, constrained by a far-field orogenic stress related to the Laurussia–Gondwana convergence process.

D_2–M_2 lower gneiss unit

The LGU covers most of the PSGD, whose lowest crustal levels are currently exposed at the surface. While the highest metamorphic grade is found here it was previously mapped as Precambrian basement and as 'Hercynian' (i.e. Variscan) alkaline igneous rocks by Galopim de Carvalho *et al.* (1981). The LGU is mostly composed of quartzofeldsphatic gneiss interlayered with paragneiss and sillimanite + garnet biotiteschist, marble, rare amphibolite and black metachert. It includes many variably foliated granitic rocks (i.e. felsic partial melts) and granitic aplite–pegmatite veins and dykes, which are concordant or discordant to the pervasive S_2 foliation (Fig. 6). The LGU lithological association resembles the Ediacaran to Cambrian stratigraphy of other less deformed and metamorphosed OMZ regions. Thus, it seems likely that the sedimentary and volcanic rocks of the Ediacaran Serie Negra Group, the Cambrian series composed of siliciclastic and carbonate sedimentary rocks and volcano-sedimentary complexes of bimodal composition, as well as Cambrian granitic plutons (in accordance with the new ages obtained and discussed below), were all transformed into LGU metamorphic rocks under M_2 amphibolitic conditions.

The LGU is defined by the sillimanite + K-feldspar metamorphic zone representing high-amphibolite facies metamorphism (Figs 4–7 and 8g–j). LGU mylonitic paragneisses are mostly composed of quartz and feldspar and are interlayered with biotite schist containing syn-D_2 fibrolite and garnet porphyroblasts (Fig. 6). Sillimanite is replaced by pre- to syn-D_3 sericite and large crystals of white mica (Fig. 6d, i). Mylonitic orthogneiss (including the Valongo orthogneiss) (Figs 6k, l and 8a–f) showing S_2 foliation and consisting of quartz, K-feldspar (microcline), plagioclase (albite), biotite, muscovite and rare amphibole, occurs interlayered with mica schist, sometimes resembling an arkosic quartzite, and amphibolite, and is intruded by variably foliated concordant and discordant dykes and veins of granitic pegmatite–aplite rocks (Fig. 6e, f and h). Amphibolite foliation is defined by alternating layers enriched with brown hornblende, clinopyroxene and sphene, and plagioclase–quartz-rich layers (Fig. 8g–j). Close to the contact with the ISU, clinopyroxene is absent in amphibolite and brown hornblende is replaced by bluish-green hornblende and biotite (Fig. 8i), suggesting a decrease in the grade of metamorphism towards the top of the LGU. The LGU paragneiss and amphibolite commonly show intrafolial folds with axial plane S_2 and axes parallel with and perpendicular to Le_2 stretching lineation. Felsic veins with abundant quartz and albite–K-feldspar, and granitic pegmatite–aplite veins concordant and discordant to the S_2 foliation are likely the product of partial melting.

D_2–M_2 intermediate schist unit

The ISU is tectonically located between the LGU and the USU (Figs 3–5). A late-D_2 brittle-ductile high-angle extensional shear zone (i.e. the Seda shear zone) crosscuts the earlier D_2 low-angle extensional shear zones and M_2 metamorphic isograds (Figs 4 and 5). The Chancelaria orthogneiss exposed along an NW–SE-trending mylonitic band 8 km long and 1 km in width NW of Seda probably represents the base of the ISU (Fig. 3). It consists of quartz, K-feldspar (microcline), plagioclase (albite–oligoclase), biotite and muscovite (Fig. 8c). It shows a coarse-grained texture and is crosscut by the development of discrete and anastomosed shear zones showing mylonitic foliation.

The ISU, composed of mica schist and metagreywacke, marble, black metachert and quartzite, assigned to the Ediacaran Serie Negra Group, is exposed along with its contact with the LGU (Figs 3 and 5). Two subunits corresponding to different metamorphic zones are distinguished based on the mineral assemblages of the ISU mica schist (Figs 7, 9 and 10a–e). The sillimanite zone represents the lower subunit of the ISU, composed of mica schist with early to syn-D_2 staurolite and garnet porphyroblasts mantled by S_2 mylonitic foliation and showing syn-D_2 mica fish of biotite indicating sense of shear towards SE–ESE (Fig. 9a–f). The white mica of the matrix is fine-grained and defines the S_2 foliation. It partially replaces fibrolite and also shows a polygonal shape, developing over S_2 foliation. Coronas of chlorite or sericite surrounding garnet porphyroblasts are common and, in some cases, biotite occurs as asymmetric pressure shadows on garnet (Fig. 9c–e). Staurolite exhibits euhedral twin-shape (Fig. 9b, c) and internal complex structures. It shows a core including weakly oriented to wavy inclusion trails of opaque minerals and quartz defining an earlier foliation (S_1) that is folded developing a spaced S_{2a} foliation, surrounded by a rim with inclusion trails parallel to the later S_2 foliation (Fig. 9c, e and f). Staurolite is in contact with or includes garnet surrounded by a corona of sericite (Fig. 9b). Garnet within staurolite porphyroblasts occurs as non-oriented or weakly oriented grains, whereas garnet in the matrix shows oriented inclusion trails and pressure shadows of quartz, biotite and white micas that are subparallel or slightly rotated and become subparallel to the S_2 foliation (Fig. 9e, f). The ISU sillimanite zone is not represented to the east of Galveias (Fig. 4), suggesting that it was removed by an early D_2 extensional shear zone separating the ISU from the USU in this area.

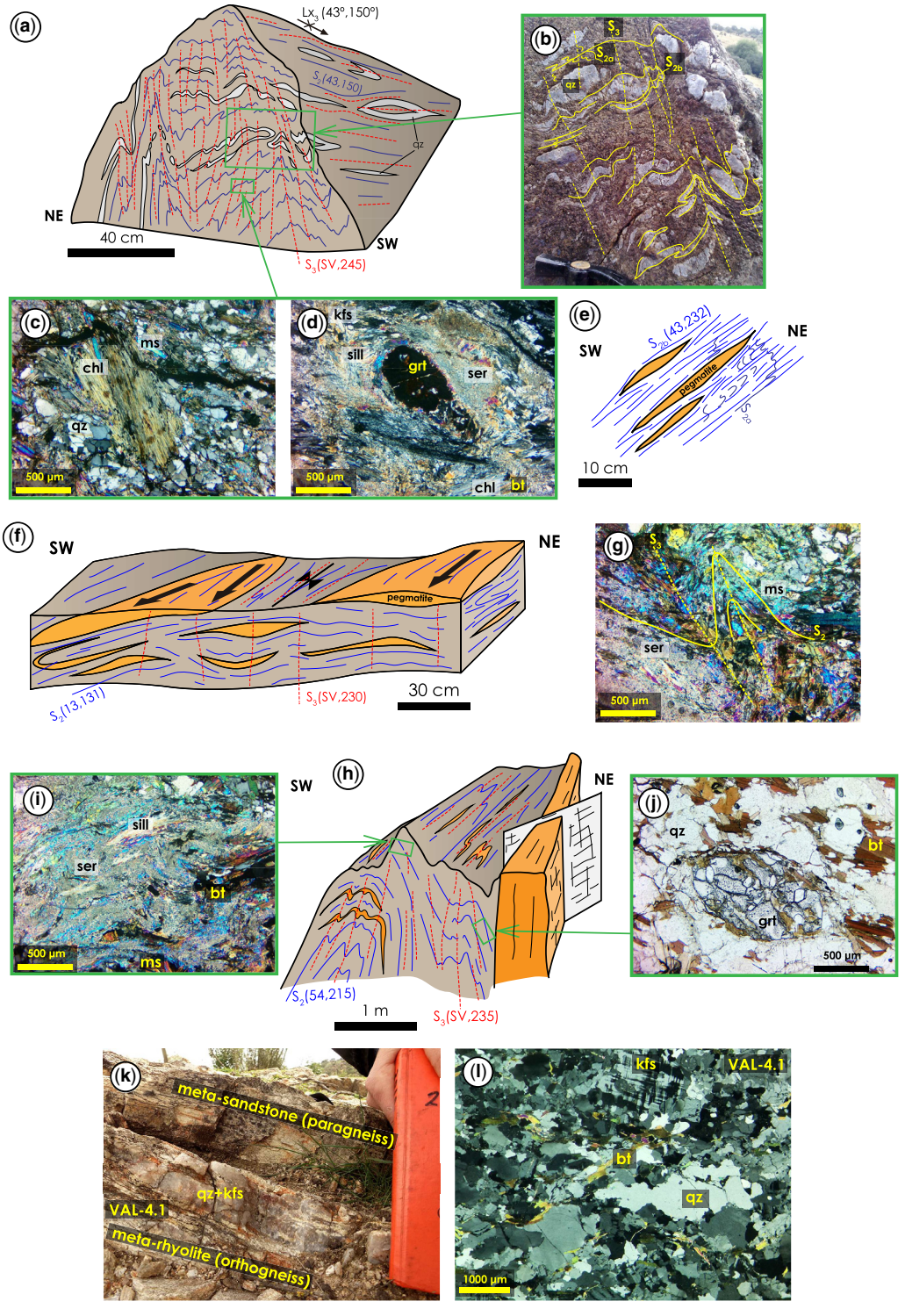
(a)
Lx3 (43°,150°)
S3(43,150)
qz
NE
SW
40 cm
S3(SV,245)
(b)
S3
S2a
S2b
qz
(c)
ms
chl
qz
500 µm
(d)
kfs
sill
grt
ser
chl
bt
500 µm
(e)
S2b(43,232)
NE
SW
pegmatite
S2b
10 cm
(f)
SW
NE
pegmatite
S2(13,131)
S3(SV,230)
30 cm
(g)
S3
ms
S2
ser
500 µm
(h)
SW
NE
S2(54,215)
1 m
S3(SV,235)
(i)
sill
ser
bt
500 µm
ms
(j)
qz
bt
grt
500 µm
(k)
meta-sandstone (paragneiss)
qz+kfs
VAL-4.1
meta-rhyolite (orthogneiss)
(l)
kfs
VAL-4.1
bt
qz
1000 µm

The andalusite–staurolite–garnet zone (second andalusite zone) is defined in the uppermost subunit of the ISU by the occurrence of mica schist with porphyroblasts of skeletal to subhedral andalusite. These metamorphic rocks are exposed in Seda and in the direction of and to the east of Galveias (Figs 3, 4, 9g–k and 10a–e). The ISU lithological association described as the Santo António volcano-sedimentary complex is assigned to the Middle–Upper Cambrian by Galopim de Carvalho *et al.* (1981) whereas in Galveias it is comparable to the Ediacaran Serie Negra Group. In both cases, skeletal andalusite porphyroblasts and snowball staurolite porphyroblasts of mica schists are mantled and cut by S_2 foliation (Fig. 10d, e). This foliation is defined by the alignment of fine- to coarse-grained mica fish and dynamically recrystallized quartz. Intrafolial folds are commonly isoclinal and show discrete foliation subparallel to the axial plane and S_2 foliation (Figs 9g–k and 10b). Mica fish of biotite and sigma-shaped staurolite porphyroblast preserving a folded S_1 or S_{2a} foliation indicate a dominant top-to-the-SE–ESE shear sense (Fig. 10e), while S–C fabric and C' shear planes with contrasting kinematics are also found. Syn-D_2 biotite porphyroblasts show local retrogradation to chlorite or to sericite and oxides, while their original shape is preserved. Close to the non-deformed granite that crops out west of Galveias (Fig. 10a, b), a new generation of post-D_2 chlorite porphyroblasts occurs along the zone of contact with metamorphic aureole.

D_2–M_2 upper slate unit

The USU is divided into three subunits defining different metamorphic zones separated by early D_2 extensional shear zones (Figs 4, 5 and 7). A steep 70° east-dipping late-D_2 normal brittle-ductile shear zone (Fig. 9a) running from Seda to the south (i.e. the Seda shear zone) defines the tectonic contact of the ISU and the USU, which crosscuts earlier D_2–M_2 fabrics and metamorphic isograds. The lowest subunit of the USU is exposed SE of Valongo in the Cambrian Santo António volcano-sedimentary complex near Benavila. The lithological association of felsic and mafic metavolcanic rocks, marbles and calcschists occurs with black to dark-grey slates with euhedral chiastolite porphyroblasts. Chiastolite ranging from 1 to 5 cm long is most abundant in the most pelitic and darker layers, representing the first andalusite zone (Fig. 10f–h). S_2 foliation is well developed in the fine-grained slaty phyllosilicate-rich matrix and occurs flowing around chiastolite porphyroblasts. Andalusite also shows an internal rotated foliation (S_{2a}) suggesting syn-kinematic growth (Fig. 10f–h). Banded amphibolite is associated with banded marble, both of which present lighter layers with granoblastic texture composed of calcium-rich silicate minerals such as garnet, diopside, amphibole, epidote, titanite and plagioclase. An abundance of epidote and bluish-green hornblende suggests that this volcano-sedimentary complex underwent low-amphibolite facies metamorphism during M_2.

Towards the top of the USU, the intermediate subunit is defined by the biotite zone that is exposed in the Santo António volcano-sedimentary complex. It is confined to a narrow band composed of metapelites and metafelsic volcanic rocks that commonly show a granoblastic texture and are mostly composed of an assemblage of quartz, feldspar, biotite

Fig. 6. Field and petrographic aspects of the LGU metapelitic rocks and relationship with granitic veins. (**a**) Field observation-based 3D sketch of sillimanite–K-feldspar–biotite-rich mica schist and paragneiss (GPS, UTM WGS84 29S: $X = 591\ 134$; $Y = 43\ 43\ 186$). D_3 shortening superimposed on flat-lying S_2 foliation and intrafolial folds defined by quartz veins with K-feldspar. (**b**) Detail of (a) showing the field relation between D_2 and D_3 fabrics. (**c**) and (**d**) Thin-section views (cross-polarized light) showing S_2 foliation defined by the alignment of fine-grained biotite (bt), quartz (qz) and K-feldspar (kfs); note a strongly chloritized (chl) porphyroblast of syn-D_2 biotite (bt) with zircon inclusions and a porphyroblast of syn-D_2 garnet (grt) showing a corona of sericite (ser), involved in a fine-grained matrix with fibrolite (sill) partially replaced by sericite. (**e**) Field observation-based 2D sketch showing mica schist with granitic pegmatite veins cutting S_{2a} and transposed by S_{2b} foliation. (**f**) Field observation-based 3D sketch of mica schist (GPS: 591 685; 43 43 489) showing flat-lying S_2 foliation and its relationship with granitic pegmatite-aplite syn-D_2 veins (i.e. felsic partial melts) and intrafolial folding suggesting top-to-SE sense of shear (black arrows). (**g**) Thin-section view (cross-polarized light) of sillimanite–biotite-rich mica schist (GPS: 592 512; 43 43 102) showing S_3 foliation (i.e. crenulation cleavage) formed by shortening and folding of a previous S_2 foliation. (**h**) Field observation-based 3D sketch of mica schist and paragneiss (GPS: 591 202; 43 42 544) showing syn-D_2 concordant granitic pegmatite veins folded by D_3 shortening, cross-cut by a discordant granitic pegmatite-aplite dyke; note that this dyke is cut by a late D_3 brittle-ductile fault. (**i**) and (**j**) Thin-section views of mica schist (cross-polarized light) showing the high-grade biotite–sillimanite-rich foliated matrix retrogressed to muscovite (ms) and sericite during D_3; porphyroblast of syn-D_2 garnet with poorly oriented inclusion trails embedded in a matrix composed of quartz, feldspar and biotite. (**k**) Foliated quartzofeldspathic orthogneiss (sampling site of the Valongo orthogneiss, VAL-4.1, for U–Pb geochronology) showing concordant syn-D_2 veins composed of quartz and K-feldspar (GPS: 598 304; 43 40 269). (**l**) Thin section (cross-polarized light) of sample VAL-4.1 that was analysed for geochronology showing the textural features of a meta-igneous rock preserving quartz and K-feldspar porphyroclasts.

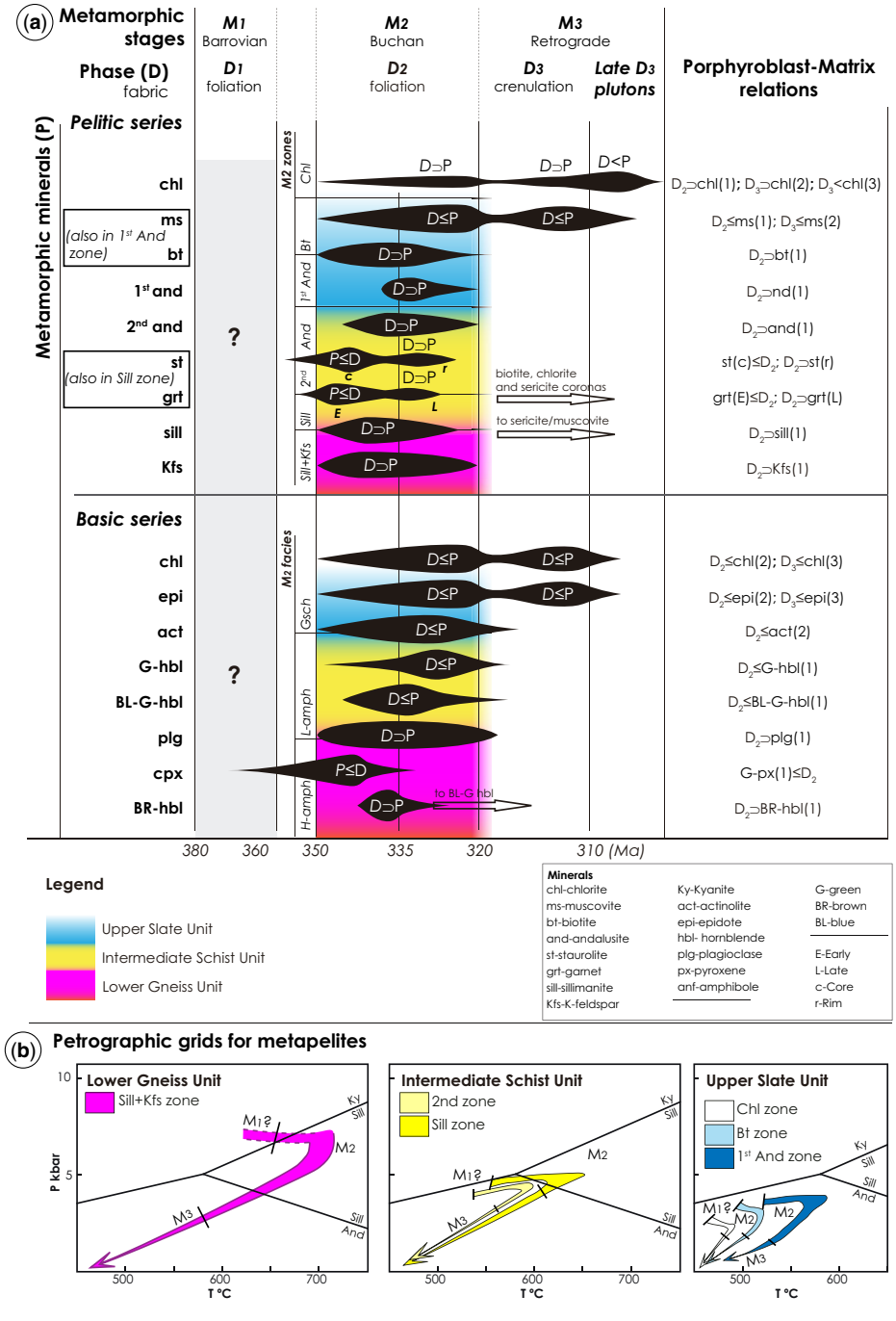

Fig. 7. (**a**) Summary of the petrographical relationships between mineral phases (P) and fabrics (D) in metapelitic and metabasic rocks in the Ponte de Sor–Seda gneiss dome: P, mineral; D, deformation stage; P < Dn, pre-tectonic with respect to Dn; P ≤ Dn, pre- to syn-tectonic; Dn ⊃ P, syn-tectonic; Dn < P < Dn + 1, inter-tectonic; Dn ≤ P, syn- to post-tectonic; Dn < P, post-tectonic. (**b**) Pressure–temperature (*P–T*) diagrams for the tectono-metamorphic units LGU, ISU and USU showing the relationship between the M_2 (D_2 crustal extension) and M_3 (D_3 crustal shortening) metamorphic events. Source: in (a), the fabric–porphyroblast nomenclature is after Rubenach and Bell (1988) and Passchier and Trouw (2005). (b) Based on Spear (1995).

and opaque minerals (Fig. 8k). These low-grade metamorphic rocks are foliated or weakly recrystallized while preserving igneous textures (Fig. 8l), locally affected by intense carbonatization. The uppermost subunit of the USU is composed of the lower-grade metamorphic rocks (Silurian–Devonian 'Xistos Raiados' Formation; Ferreira and Piçarra 2020) defining the chlorite zone. The subunit includes silky slates rich in quartz, chlorite, sericite, tourmaline and iron oxides (described as phyllites by Galopim de Carvalho *et al.* 1981) of greenschist facies metamorphism. It comprises mostly slates and also metagreywackes, black metacherts and graptolitic slates (Gonçalves 1973), and locally contains intrafolial folds.

D_3–M_3 structure

The D_3–M_3 structure in the PSGD is characterized by general NW–SE upright and open folds, locally with tight disharmonic folding affecting S_2 foliation (Figs 6a, b, g, h and 10c). D_3 contractional deformation led to the steepening of the D_2–M_2 fabric within the limbs of isoclinal D_3 folds and along brittle-ductile transpressive shear zones, such as those located to the north of the PSGD (Figs 4 and 5). The axial planar cleavage of the D_3 folds has a mean direction of 80°/234°, and the fold axes and interception lineation have a mean principal direction of 32°/148° (Fig. 4). Unfolding around this axis, which is approximately the same as the beta axis of the D_2 fabric, the S_2 foliation gradually becomes gently dipping towards the ESE before D_3. The general replacement of sillimanite and andalusite with post-S_2 muscovite may be related to M_3 retrograde metamorphism as described for the Évora gneiss dome (Dias da Silva *et al.* 2018). Decreasing temperature is also evidenced by the chloritization and sericitization of coronas of garnets, as well as the growth of epidote and sphene in LGU and ISU amphibolites (Fig. 7).

Zircon U–Pb geochronology

Mylonitized felsic meta-igneous rocks from the base of the ISU (sample CHA-2, Chancelaria orthogneiss; GPS: UTM WGS84 29T; $X = 601\,785$; $Y = 43\,44\,546$) and the LGU (sample VAL-4, Valongo orthogneiss; GPS: 598 339; 43 40 235) were selected for U–Pb zircon geochronology (see Figs 3 and 5 for locations). The results of U–Pb SHRIMP analyses are listed in the Supplementary material. Concordia diagrams are shown in Figure 11

Analytical method

Two representative zircons groups (CHA-2.1, $n = 55$; VAL-4.1, $n = 64$) were mounted in epoxy together with the TEMORA standard (Black *et al.* 2003) and polished to attain quasi-central sections that were used for radiogenic isotope and rare earth element (REE) analysis. Later, the polished mounts were Au-coated for examination using a FEI-QUANTA 250 scanning electron microscope equipped with secondary-electron, cathodoluminescence (CL) detectors and electron dispersive spectroscopy (EDS) Oxford X-Max 80 model, at IGc-CPGeo, at the University of Sao Paulo (USP). CL imaging was carried out under the following conditions: 60 μA of emission current, 15.0 kV of accelerating voltage, 6 μm of beam diameter, 18 mm of work distance, 60 μs of acquisition time and 2048 × 1768 px of image resolution.

Isotope measurements were performed using a SHRIMP-IIe (IGc-CPGeo, USP), following the analytical procedures used previously (Williams 1997; Sato *et al.* 2014). Uranium abundance and U–Pb ratios were calibrated against the TEMORA standard (Black *et al.* 2003), and age calculations were performed using Isoplot© 3.0 (Ludwig 2003). SHRIMP-IIe analysis was carried out under the following set-up conditions: spot size = 30 μm, mass resolutions for $^{196}(Zr_2O)$, ^{206}Pb, ^{207}Pb, ^{208}Pb, ^{238}U, $^{248}(ThO)$ and $^{254}(UO)$ ranging from 5,000 and 5,500 (1%), and residues <0.025 (Sato *et al.* 2014).

All the data presented in the concordia diagrams were corrected for common Pb using the ^{208}Pb correction method (Williams 1997). Error data are reported at the 1σ level, except where otherwise indicated.

Results

The analysed zircon population of the Chancelaria orthogneiss (sample CHA-2.1, Fig. 8c) contains subhedral to prismatic euhedral grains (60–200 μm in diameter). Prisms are slightly to markedly elongate, with a simple internal structure characterized by banded or concentric zoning, in some cases surrounded by a very thin dark rim (Fig. 11). A total of 30 U–Pb SHRIMP analyses for sample CHA-2.1 yielded an average Th/U ratio of 0.36, which is a typical indicator of igneous origin (Heaman *et al.* 1990; Hanchar and Miller 1993; Hoskin and Schaltegger 2003), and precipitation from felsic-intermediate metaluminous sources. After correction for ^{204}Pb, most zircon ages are located near the concordia line and scattered in the range *c.* 645–506 Ma (Fig. 11a), while the remaining more recent ages are relatively more discordant. This dataset ($N = 30$) was used to obtain an intercept age of 555 ± 36 Ma (mean square weighted deviation, MSWD = 0.04; Fig. 11a). Analyses from the same composite grain with a 'disturbed' core (analysis 7.1 and 10.1, both probably more affected by

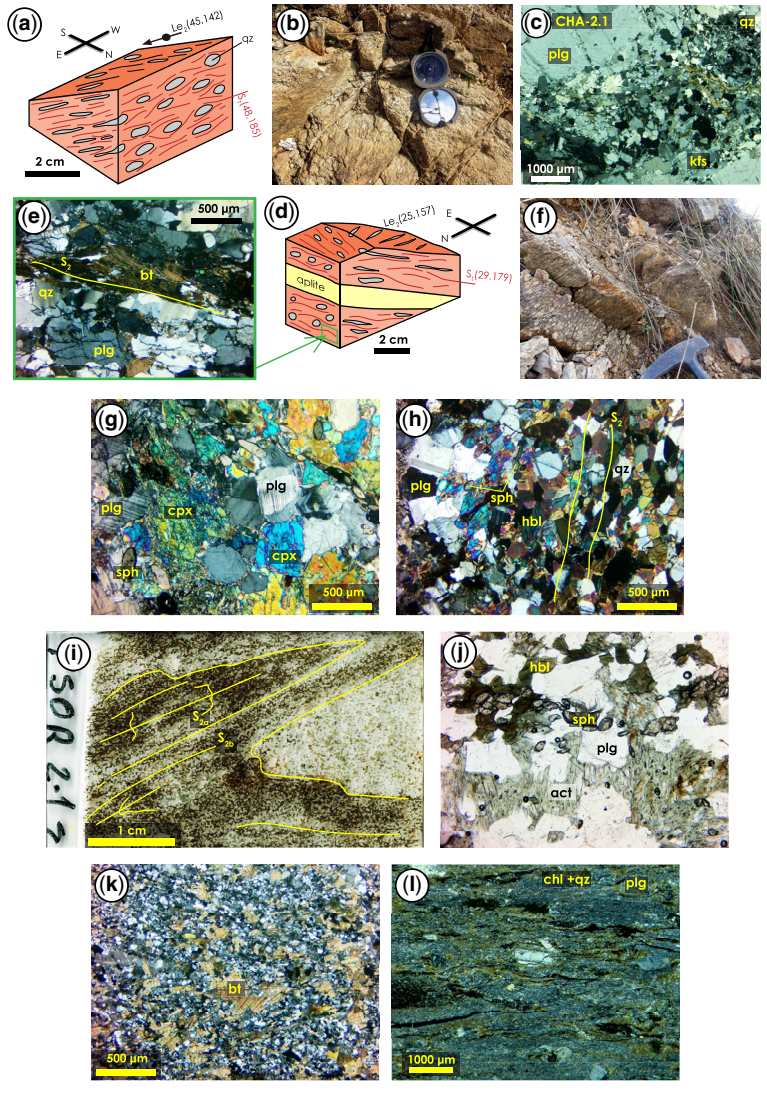

Fig. 8. Field and petrographic aspects of meta-igneous rocks from the Ponte de Sor–Seda gneiss dome. (**a**) Field observation-based 3D sketch showing the coarse-grained foliated LGU orthogneisses (GPS: 595 093; 43 42 080) that is parallel to S_2 foliation of the surrounding mica schist. The stretching lineation (L_e) is mainly defined by elongate phenocrysts of quartz. (**b**) Coarse- to medium-grained quartzofeldspathic orthogneiss shown in (a). (**c**) Petrographic aspect of the Chancelaria (augen) orthogneiss (sample CHA-2.1) having large plagioclase (plg) and K-feldspar (kfs) porphyroclasts mantled by a highly recrystallized quartz + biotite + K-feldspar matrix (GPS: 601 785; 43 44 546). (**d**) Field observation-based 3D sketch showing the relationship between the foliated coarse-grained LGU orthogneiss and concordant syn-D_2 granitic aplite veins (Fig. 8f; GPS: 595 093; 43 42 080). (**e**) Thin-section view of the quartzofeldspathic orthogneiss in (d) and (f) (cross-polarized light) showing elongated grains of quartz with undulose extinction and subgrains, plagioclase (plg) with undulose extinction, and biotite defining S_2 foliation. (**f**) Coarse-grained foliated quartzofeldspathic orthogneiss. (**g**) and (**h**) Thin-section views of LGU amphibolite (cross-polarized light) showing weakly oriented clinopyroxene (cpx), plagioclase and sphene (sph) (GPS: 591 380; 43 43 250) or elongated brown hornblende (hbl) and plagioclase defining the S_2 foliation (GPS: 591 153; 43 43 270). (**i**) Naked-eye observation-based 2D sketch of a thin-section of LGU amphibolite (GPS: 591 280; 43 43 335) showing a D_2 intrafolial fold. S_{2a} layering/foliation is folded and transposed by S_{2b}, showing that both S_2 foliations developed during D_2 progressive extensional deformation. (**j**) Thin-section view of LGU amphibolite (parallel-polarized light) described in (i) showing brown hornblende, sphene, plagioclase and actinolite (act) replacing hornblende or clinopyroxene. (**k**) Thin-section view of fine-grained ISU metadioritic rock (Santo António volcano-sedimentary

Pb-loss) surrounded by an 'older' overgrowth (analysis 7.2 and 10.2), one analysis with discordance >10% (6.1), and the three oldest grains (*c.* 645, 592 and 585 Ma; Neoproterozoic), which are interpreted as being xenocrysts, were excluded from the age calculation. The 11 grains in the $^{208}Pb/^{238}U$ age range *c.* 548–526 Ma (^{204}Pb-corrected and discordance <10%) yielded a concordia age of 539 ± 2 Ma (MSWD = 0.23; Fig. 11b), which is the best estimate for the protolith age (Late Ediacaran–Early Terreneuvian) of Chancelaria orthogneiss.

CL imaging shows that zircon grains (50–150 μm in diameter) in the Valongo orthogneiss (sample VAL-4.1, Fig. 6k, l) are stubby to elongate euhedral with well-developed crystal faces, mostly with oscillatory growth, and very long prisms with a length–width ratio reaching 5:1, with banded zoning (Fig. 11). Some grains show a very thin dark rim, whereas others are partly resorbed. Zircon grains have an average Th/U ratio of around 0.31, which is comparable with the value obtained for sample CHA-2.1. From the plotting of 31 analyses in the Tera–Wasserburg diagram, we obtained an intercept age of 536 ± 16 Ma (MSWD = 0.36) (Fig. 11c). A total of 11 analyses with discordance >10%, including analyses from the same composite grain (3, 5 and 9) with a 'disturbed' core surrounded by an 'older' overgrowth, were not considered for concordia age interpretation because they probably experienced Pb-loss. The oldest grains scattered along the concordia line in the $^{208}Pb/^{238}U$ age range *c.* 583–508 Ma (^{204}Pb-corrected and discordance <10%) represent Ediacaran to Cambrian xenocrysts (Fig. 11c), overlapping the Late Ediacaran–Early Terreneuvian ages found in the xenocrysts of sample CHA-2.1. Four analyses with discordance of <10% (4.1, 12.1, 13.1 and 16.1), which are the youngest ages, yield a concordia age of 496 ± 3 Ma (MSWD = 1.4; Fig. 11d), representing the best estimate of the protolith age (Late Miaolingian–Early Furongian) of the Valongo orthogneiss.

Discussion

Tectonic model for Variscan crustal extension in the OMZ

Gneiss domes may result from large-scale crustal flow (Whitney *et al.* 2004) under high-temperature conditions at variable depths, due to extensional tectonics that triggers crustal thinning, decompression and partial melting (Rey 1993; Teyssier and Whitney 2002). The development of gneiss domes may contribute decisively to the rapid exhumation of the orogenic roots in a convergent plate boundary (Lister *et al.* 1984). In such convergent tectonic settings, slab rollback can cause crustal uplift in the upper plate below low-angle extensional shear zones (i.e. detachments) in gneiss domes (Jolivet and Brun 2010). Indeed, retreating subduction can lead to significant crustal extension of the overriding plate and the formation of a backarc basin (Cawood *et al.* 2009). Numerical models of slab rollback and trench retreat have demonstrated that delamination of the lower crust and lithospheric mantle tend to occur concurrently or after collision (Ueda *et al.* 2012). Furthermore, the early stages of collision may be accommodated by the subduction of the lower crust and mantle lithosphere beneath the overriding plate, followed by a retreat from the collision zone (Gray and Pysklywec 2012). As a consequence of this kind of tectonic instability of the mantle, the lithosphere may suffer delamination inducing decompression and partial melting (von Blanckenburg and Davies 1995). The resulting mafic magmas, which are emplaced in the thinned lithosphere of the overriding plate, cause increasing heat flow, crustal anatexis and the production of granitic rocks in mid-lower crustal levels of the orogeny (Wells and Hoisch 2008). The gradual heating of the crust may lead to thermal softening, which allows the extension typical of a gneiss dome (Brun and Faccenna 2008).

The development of flat-lying planar fabrics under metamorphic conditions reaching partial melting associated with crustal flow was a major consequence of large-scale Variscan intra-orogenic extension during the progressive assembly of Pangaea, as described for SW Iberia by Pereira *et al.* (2009). The use of the Zwart (1979) concept in relation to structural domes in the Variscan segment of the Pyrenees, consisting of a superstructure and an infrastructure, which was later revisited by Denèle *et al.* (2007), in our opinion provides a suitable framework for the reinterpretation of the tectonic evolution of the macrostructure exposed in the Ponte de Sor–Seda region (Fig. 12). The two structural domains are in this case separated not only on the basis of a great contrast between the degree of metamorphism but also on the style of deformation,

Fig. 8. *Continued.* complex) from the hanging wall of the Seda shear zone (cross-polarized light) composed of plagioclase, quartz and biotite (GPS: 605 024; 43 38 607). (**l**) Petrographic aspect (cross-polarized light) of a low-greenschist facies metabasic volcanic rock exhibiting primary textures of a welded ignimbrite with aphanitic to very fine-grained phaneritic volcanic fragments, fiammé (black opaque material) and crystal fragments (plagioclase) (GPS: 606 026; 43 39 433).

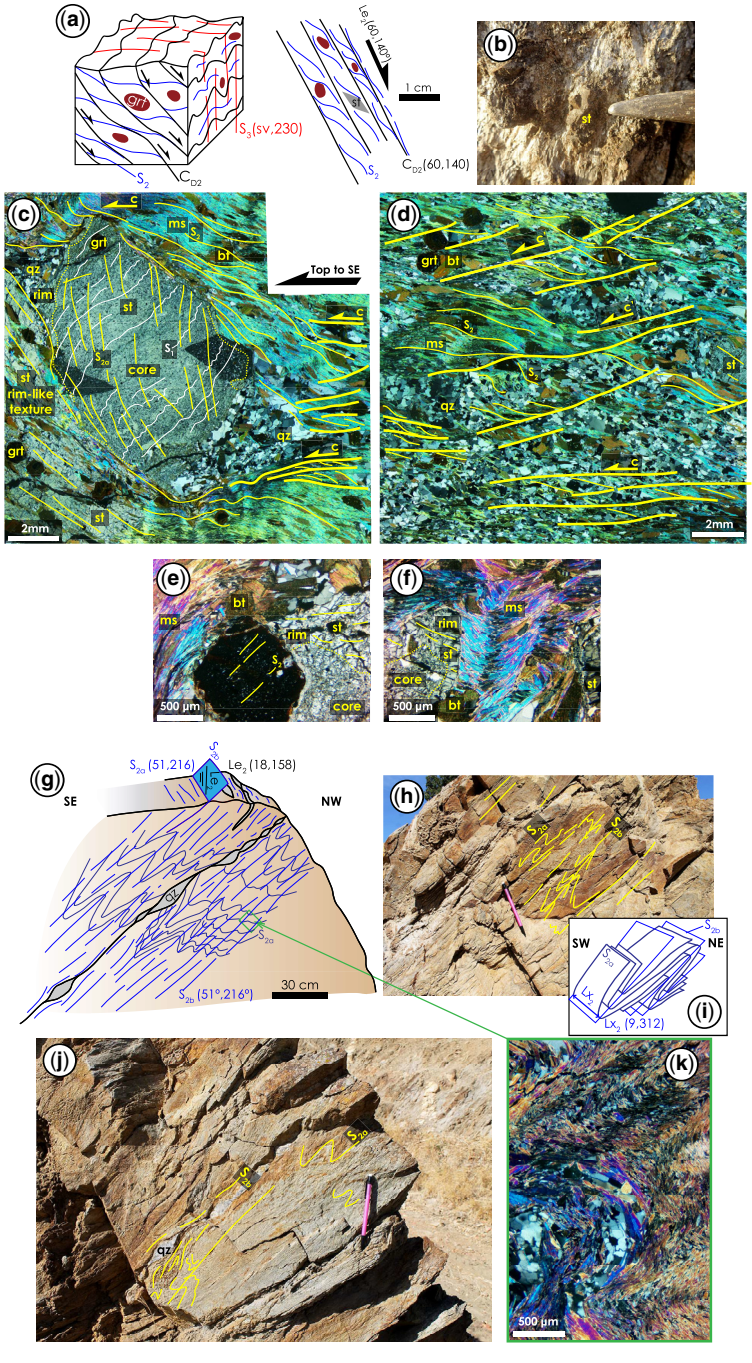

Fig. 9. Field and petrographic aspects of the ISU mica schist. (**a**) Field observation-based 3D sketch of ISU mica schist cut by the Seda shear zone (GPS: 604 255; 43 38 648). S_2 foliation is transposed by a late-D_2 high-angle S-C fabric, indicating top-to-SE sense of shear, and both D_2 structures are affected by D_3 folding. (**b**) Garnet–staurolite-rich ISU mica schist (GPS: 604 406; 43 38 450) showing a large twinned staurolite porphyroblast. (**c**) and (**d**) Thin-section views of ISU garnet–staurolite-rich mica schist (cross- and parallel-polarized light) with staurolite porphyroblasts including a folded previous foliation (S_1); these microfolds have an axial plane S_{2a} cleavage (staurolite porphyroblasts show rims of new recrystallized staurolite)

which is less pronounced close to their contact. This new perspective allows for a full understanding of the relationship between the different lithological associations and the Variscan ductile deformation, developed under low-pressure granulite to greenschist facies metamorphism, to which they were subjected. In addition, it is valuable for providing a better understanding of the evolution of the OMZ crustal architecture during the Mississippian.

The overall structural pattern of the large-scale gneiss domes of the OMZ may include an infrastructure and a superstructure, as mentioned above. The infrastructure began to form with the simultaneous development of different tectono-metamorphic units (Figs 5 and 12). The thermal anomaly moved upwards having crossed the deepest levels of the continental crust and reached shallower and more fertile crustal levels that started to partially melt. This thermal anomaly, which is responsible for the high metamorphic grade in the infrastructure, could be explained by the effects of the pressure drop associated with the high relative rate of the tectonic denudation process during crustal extension. The lower unit (core) composed of high-grade metamorphic rocks and mainly associated with variably foliated granitic rocks, including felsic partial melts (termed the MGU), was formed as a result of this dramatic rise in temperature.

A pervasive migmatitic foliation defined by a compositional layering, formed under granulite to high amphibolite facies metamorphism, characterizes the lower MGU of the Variscan OMZ infrastructure. The MGU is mainly composed of migmatite and gneiss–migmatite associated with granitic rocks (including felsic partial melts) and a few gabbro-dioritic rocks. Kinematic criteria indicate top-to-the-SE and south sense of movement. The MGU is not exposed in the PSGD but is well represented in the Évora gneiss dome, in the Aracena and Lora del Rio massifs and in the Badajoz–Cordoba shear zone (Central Unit; Fig. 1b). Geochronological data for the MGU are consistent with a Mississippian age for M_2 high-grade metamorphic rocks (*c.* 341–335 Ma; Ordóñez-Casado 1998; Pereira *et al.* 2009, 2012*b*, 2022*a*; Abati *et al.* 2018), which are temporally and spatially associated with plutonic rocks (*c.* 338–335 Ma; Moita *et al.* 2015; Pereira *et al.* 2015, 2023*b*; Rodríguez *et al.* 2022). M_2 high-temperature–low-pressure metamorphic conditions in the MGU are reported in the Évora–Aracena–Lora del Río metamorphic belt while greater pressure is recorded in the Badajoz–Cordoba shear zone (Pereira *et al.* 2012*a*). The high-grade metamorphic rocks of the Central Unit show pervasive S_2 foliation enclosing boudins of metamafic and metafelsic rocks preserving high-pressure relics (Azor *et al.* 1994; Pereira *et al.* 2010; Abati *et al.* 2018). The high-pressure metamorphic event recorded in the Badajoz–Cordoba shear zone, initially presumed to be Cadomian (Abalos *et al.* 1991), was subsequently dated at *c.* 377 Ma (upper Devonian) and therefore corresponds to the first Variscan metamorphic event M_1 reported in the OMZ (Abati *et al.* 2018; see Fig. 13a). It is assumed that these M_1 high-pressure rocks were exhumed and retrogressed during their upward path in part due to extensional shearing (Azor *et al.* 1994; Pereira *et al.* 2023*a*; see Fig. 13b–d).

The ductile shearing that was active under high-grade metamorphic conditions in the MGU developed at lower temperatures in the LGU and the ISU, indicating an abrupt change in thermal conditions, as suggested by the spatial distribution of telescoped M_2 metamorphic isograds. The MGU was tectonically overlain by an intermediate unit (LGU) composed of medium-grade metamorphic rocks and relatively less abundant granitic rocks (including partial melts) than in the MGU. Simultaneously, the ISU representing the upper unit of the infrastructure experienced ductile shearing under lower-grade metamorphic conditions along a narrow band in contact with the superstructure. Pervasive S_2 foliation

Fig. 9. *Continued.* representing inclusion trails parallel to S_{2b} (S_2 in the matrix). Sigma-shaped porphyroblasts of staurolite (with asymmetric pressure shadows filled by recrystallized quartz) and garnet, along with S–C fabric and C' shear planes and biotite mica-fish, indicate a general top-to-SE sense of shear (GPS: 604 404; 43 38 446). (**e**) and (**f**) Thin-section view of mica schist (cross-polarized light) showing porphyroblasts of garnet (grt) and staurolite (st) embedded in a foliated mica–quartz-rich matrix including sillimanite partially replaced by muscovite. Staurolite porphyroblast shows a core (first stage of st crystallization) that is surrounded by a rim (second stage of st crystallization) containing oriented inclusions of opaque minerals and biotite. Garnet porphyroblast shows straight inclusion trails subparallel to the surrounding S_2 foliation and sericite corona indicative of a retrograde reaction. Thin section made perpendicular to S_2 foliation and to the D_3 fold axis. S_2 foliation is folded by D_3 contractional event (GPS: 604 255; 43 38 647). (**g**) Field observation-based 3D sketch showing ISU mica schists from the second andalusite zone (GPS: 586 348; 43 35 506). S_{2a} foliation is folded and transposed by S_{2b} (axial plane) also marked by boudinaged quartz veins. (**h**) ISU mica schist showing D_2 intrafolial folds and the development of S_{2b} foliation (axial plane). (**i**) 3D sketch showing the spatial relationship of S_{2a} and S_{2b} observed in the photograph in (h) of ISU mica schist (L_{x2}–D_2 fold axis). (**j**) A photograph of ISU mica schist illustrated in (g) showing the relationship between the quartz vein and D_2 foliations. (**k**) Thin-section view of ISU mica schist (cross-polarized light) showing S_{2a} foliation folded and the development of S_{2b} foliation (crenulation cleavage).

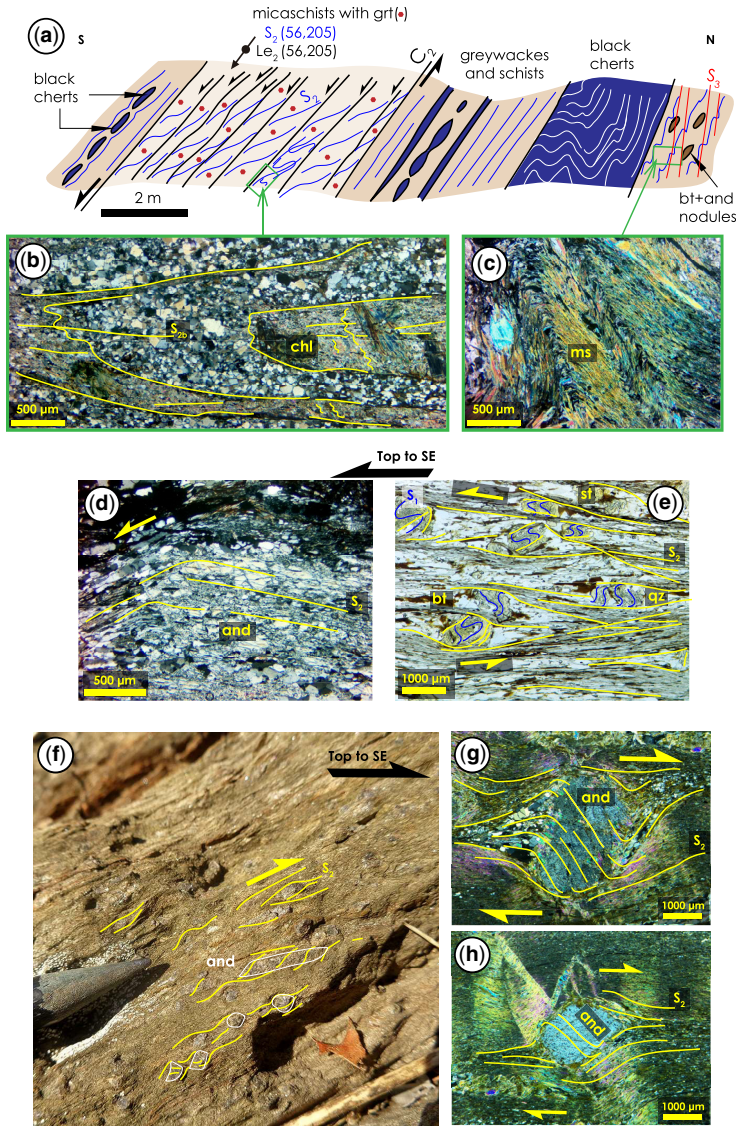

Fig. 10. Field and petrographic aspects of mica schist from the second andalusite zone of the ISU and the first andalusite zone of the USU. (**a**) Cross-section of the ISU garnet-rich micaschists, metagreywackes and black metacherts (Serie Negra Group; GPS: 586 342 43 34 780) showing boudinage and the development of S–C fabric related to D_2 extensional deformation. (**b**) and (**c**) Thin-section views of ISU garnet-rich mica schist (cross-polarized light) showing D_2 intrafolial folds with the development of S_{2b} foliation and growth of post-D_2 chlorite, and D_3 folds affecting the main S_2 foliation. (**d**) and (**e**) Thin-section views (cross- and parallel-polarized) of ISU mica schist (GPS: 591 453; 43 33 539) showing (d) sigma shape porphyroblasts of skeletal andalusite with inclusion trails rotated with respect to the S_2 foliation and (e) staurolite porphyroblasts having an earlier foliation (S_1) that is folded, surrounded by quartz–mica-rich matrix showing a well-developed S_2 fabric and syn-D_2 biotite mica-fish partially replaced by muscovite and oxides; these microstructures indicate top-to-the-SE–ESE sense of shear. (**f–h**) USU chiastolite slates (GPS: 597 935; 43 32 247), with euhedral delta (Fig. 8g) and sigma (Fig. 8e) shaped syn-D_2 andalusite prisms (first andalusite zone) growing over the S_2 foliation, indicating top-to-SE sense of shear.

and kinematic criteria indicating top-to-the-SE, south and ESE sense of shear suggest that the LGU and the ISU were tectonically juxtaposed to the partially molten MGU rocks due to the activation of a system of D_2 extensional shear zones (Fig. 12a).

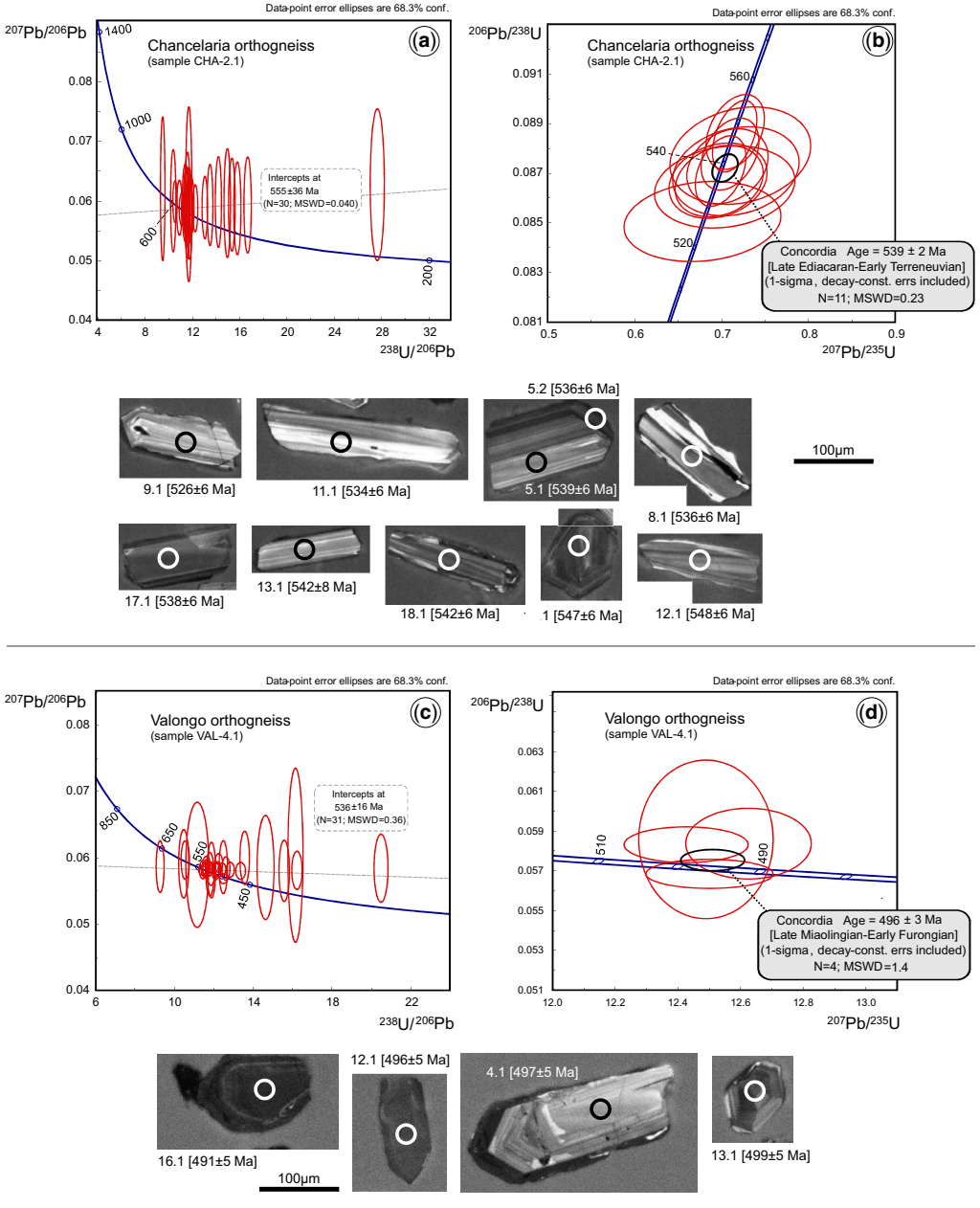

Fig. 11. Tera–Wasserburg diagram showing U–Pb data for zircon in the Ponte de Sor–Seda gneiss dome orthogneisses. Sample CHA-2.1, Chancelaria orthogneiss: (**a**) all data; (**b**) concordia age and CL-images of the youngest zircon age cluster. Sample VAL-2.1, Valongo orthogneiss: (**c**) all data, excluding analysis 8.2 and 9.2; (**d**) concordia age and CL-images of the youngest zircon age cluster. Error ellipses are drawn at 2σ.

The infrastructure is formed by the ductile crust that was exhumed by a system of D_2 low-angle shear zones. The metamorphic paths of the LGU and the USU in the Évora gneiss dome show an initial thermal increase related to S_2 foliation followed by retrogression of higher-temperature mineral assemblages, expressing the tectonic exhumation of both units (Dias da Silva *et al.* 2018). At the same time, in the uppermost crustal unit of the superstructure (USU) brittle-ductile shearing proceeded under

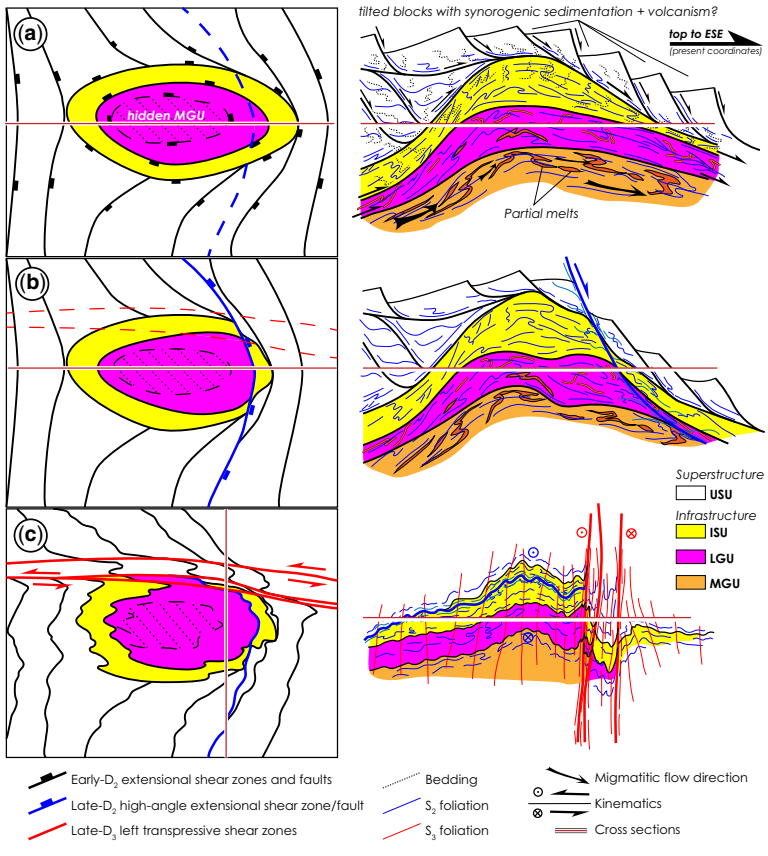

Fig. 12. Sketch maps and cross-sections of an idealized model showing the tectono-metamorphic evolution (D_2–D_3) of the Ponte de Sor–Seda gneiss dome. See text for explanation. Source: adapted from Burg *et al.* (2004) and Tirel *et al.* (2004).

low to very-low metamorphic conditions together with synorogenic sedimentation (Fig. 12a). During the final stages of the development of the Variscan gneiss dome, the exhuming ductile crust underwent progressive cooling and reached the brittle-ductile transition. As a result of this vertical movement, later D_2 high-angle shear zones, influenced by relatively lower temperatures of shearing, formed and crosscut the former telescoped metamorphic isograds (i.e. Seda shear zone; Fig. 12b). A syn-D_2 sedimentary basin may have been formed in the USU of the PSGD (Fig. 12a) due to an orogenic process similar to that described for the Évora gneiss dome (i.e. Cabrela basin; Fig. 1b) and for the French Massif Central (Montagne Noir; Brun and Van der Driessche 1994).

The structures developed prior to crustal extension are occasionally well preserved in the superstructure of gneiss domes formed after crustal thickening but are progressively erased in the deeper metamorphic units of the gneiss dome (Brun and Van der Driessche 1994). In the CIZ, D_2 low-angle extensional shear zones and the development of Variscan gneiss domes overprinting D_1 folds are recognized in the lower-grade metamorphic units (for example, Escuder Viruete *et al.* 1994; Barbero *et al.* 1995; Díez Balda *et al.* 1995; Martínez Catalán *et al.* 2003; Díaz-Alvarado *et al.* 2012; Díez Fernández and Pereira 2016; Pastor-Galán *et al.* 2019; Dias da Silva *et al.* 2021; Moreno-Martín *et al.* 2022). The same scenario is described for the OMZ (Apraiz and Eguíluz 2002) but sometimes it is almost impossible to recognize D_1 contractional structures over which the D_2 gneiss domes develop in the OMZ because D_2 extensional shearing and high-grade metamorphism may have obliterated D_1 structures in the infrastructure (Pereira *et al.* 2007, 2009; Dias da Silva *et al.* 2018). This led us to assume that the development of pre-D_2 extensional ductile fabrics may have been as weak in certain sectors of the OMZ (i.e. uppermost crustal levels of the orogenic front v. an externally orogenic region) as in the

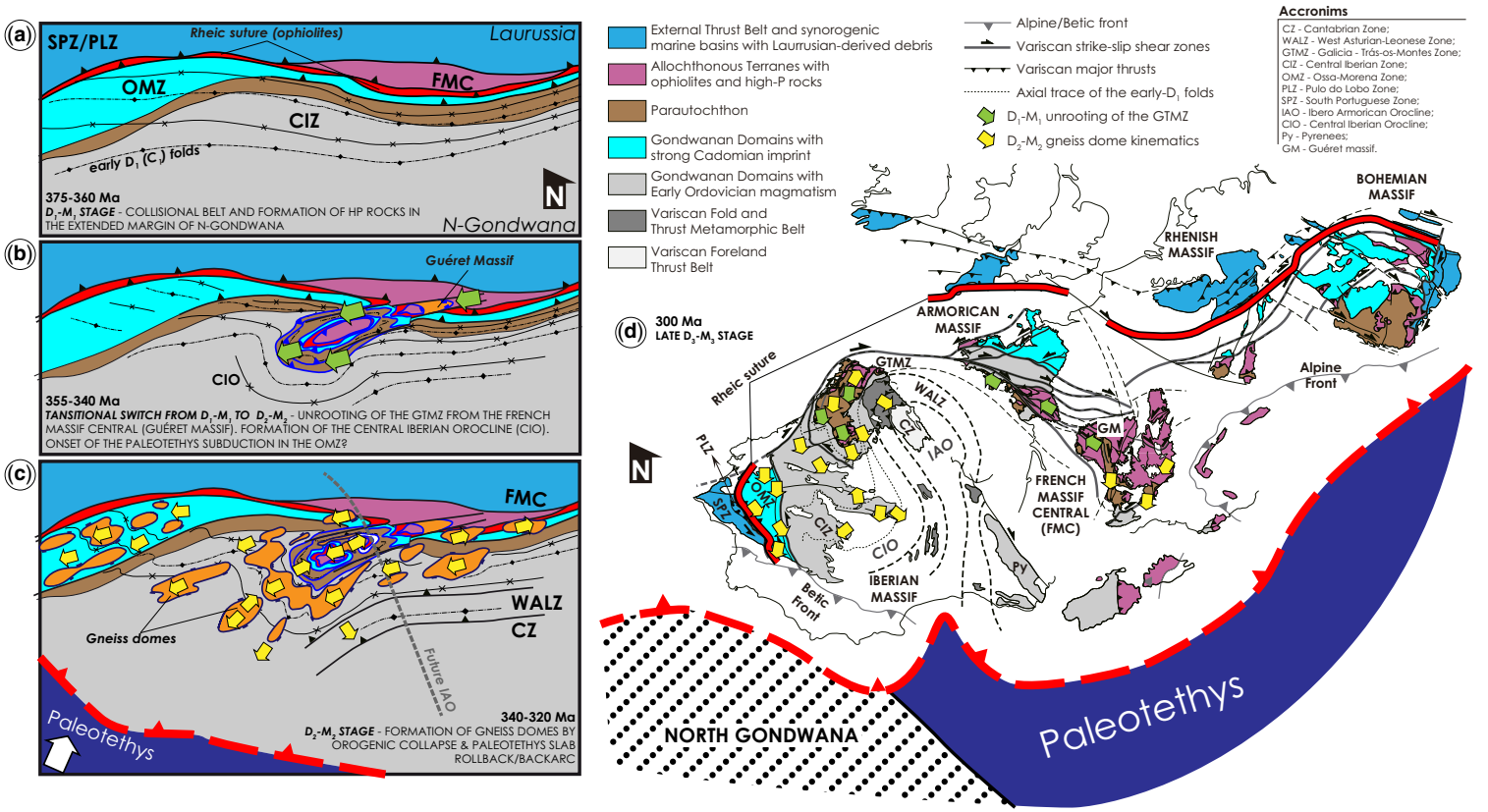

Fig. 13. Paleogeographic reconstruction and tectonic evolution of the Variscan belt illustrating the collision between Laurussia (northern continent) and North Gondwana (southern continent) and the onset of Paleotethys subduction. See text for explanation. Source: adapted from Dias da Silva (2014), Pereira *et al.* (2015), Rubio Pascual *et al.* (2016), Dias da Silva *et al.* (2021) and Martínez Catalán *et al.* (2021).

Ponte de Sor–Seda gneiss region, or practically non-existent.

The switch from D_2 extension to D_3 contractional deformation renewed crustal shortening. NE–SW oriented shortening (present-day coordinates; Figs 1 and 13) is reflected by the D_3 transpressive shear zones and upright folding. Higher-grade tectono-metamorphic units of the PSGD experienced folding together with lower-grade domains to define the current upright folded structural architecture of the study region (Fig. 12c).

The structuring of the continental crust due to extensional tectonics impacted not only the OMZ but also other regions of the European Variscan orogenic belt, such as the French Massif Central, the Iberian and Bohemian massifs, the Vosges (Rubio Pascual *et al.* 2016; Vanderhaeghe *et al.* 2020, and references therein) and the Pyrenees (Denèle *et al.* 2007), all representing North Gondwana remnants of the Pangaea supercontinent (Fig. 13). Most authors who have developed tectonic models for the evolution of the Variscan orogenic belt agree that a regional thermal anomaly facilitated the development of the flat-lying planar ductile fabrics and the onset of gneiss domes during crustal extension (Simancas *et al.* 2003; Faure *et al.* 2009; Pereira *et al.* 2009; Alcock *et al.* 2015; Gapais *et al.* 2015; Martínez Catalán *et al.* 2021; Schulmann *et al.* 2022, and references therein). As an alternative, the development of flat-lying foliation might reflect gravity-driven lateral flow of the thickened and thermally weakened orogenic crust forming an orogenic plateau (e.g. Vanderhaeghe *et al.* 2003; Vanderhaeghe 2009, 2012). However, a number of different causes have been proposed for explaining the triggering mechanism for this large-scale thermal anomaly. Transition from crustal thickening to gravitational collapse of the Variscan belt during convergence and regional extension constitutes the most likely tectonic model for the French Massif Central and the Pyrenees (Costa and Rey 1995). The gravitational collapse of the Variscan orogen was accommodated by extension of the upper crustal levels and by lateral flow and exhumation of the partially molten lower crustal levels, leading to the formation of crustal-scale gneiss domes (Vanderhaeghe *et al.* 2020). The protracted melting of the root of the Variscan orogenic crust was probably produced by the effects of an increase in radioactive heat production in the thickened crust, combined with an increase in mantle heat flux owing to lithospheric mantle thinning beneath the Variscan orogen (Vanderhaeghe and Duchêne 2010; Schulmann *et al.* 2022). The thermal anomaly recorded in the OMZ has been interpreted as resulting from the emplacement in middle crustal levels of voluminous mantle plume-related magmas (Simancas *et al.* 2009). Additionally, the onset and development of this large-scale thermal anomaly may have been caused and magnified, respectively, by the Paleotethys oceanic lithosphere beneath the OMZ (Pereira *et al.* 2020*a*, *b*; Rodríguez *et al.* 2022; Fig. 13b–d).

It is also possible that subduction of the Paleotethys oceanic lithosphere may not have caused dramatic heat flow in the North Gondwana continental margin. A tectonic model designed for the evolution of the French Massif Central during the Carboniferous (*c.* 345–310 Ma) posits the development of an orogenic plateau by lateral flow of the partially molten orogenic root in a context of plate convergence and southward slab retreat of the Gondwana megaplate (Vanderhaeghe *et al.* 2020). According to Vanderhaeghe *et al.* (2020), subduction and partial melting of the North Gondwana continental margin may explain the voluminous granitic magmas along with mafic magmas probably derived from mantle melting caused by decompression as a consequence of slab retreat.

Another tectonic model, developed by Franke (2014), supports the possible existence of a mantle plume leading to the presence of a lithologic association of mafic rocks (sills) interspersed with metamorphic rocks in the OMZ middle crust (i.e. Iberian Reflective Body; Simancas *et al.* 2003). In accordance with this model, the high-temperature regime was not connected, in time and space, with continental collision but instead occurred in response to the propagation of the Paleotethys Rift across the Late Paleozoic orogen, and explains the dramatic profuse high heat flow and contamination of Mississippian magmas.

Long-term Cambrian magmatism and crustal recycling in the OMZ (North Gondwana margin)

The Cambrian ages calculated for the protoliths of the PSGD (Valongo and Chancelaria) orthogneisses provide a significant contribution to the updating of the Geological Map of Portugal and improving our overall knowledge of Paleozoic magmatism in the OMZ. These igneous rocks, which have been associated with the Variscan orogeny (i.e. 'Hercynian'; Galopim de Carvalho *et al.* 1981), are older, and are associated with the protracted evolution of the North Gondwana continental crust long before the onset of the Mississippian gneiss domes.

The new age obtained for the protolith of the Chancelaria orthogneiss (538 $\pm$ 2 Ma; this study) coincides with the time interval associated with the initial stages of North Gondwana continental margin extension during Terreneuvian arc-rift transition, following Ediacaran crustal accretion. The protolith age of Chancelaria orthogneiss either coincides with

or approaches the protolith age range of Terreneuvian OMZ andesites dated at 534 ± 4 Ma (the Malcocinado Formation; Sarrionandia *et al.* 2020), and Monestério and Mina Afortunada migmatites dated at 533 ± 4 Ma and 532 ± 4 Ma, derived from the partial melting of the Ediacaran Serie Negra Group (Ordóñez-Casado 1998; Sánchez-García *et al.* 2008). Terreneuvian to Cambrian-Series 2 magmatic activity is further represented in the OMZ by younger volcanic and plutonic rocks dated at 530 ± 3 Ma (Cala rhyolitic porphyry; Romeo *et al.* 2006), 526 ± 10 Ma (Alcáçovas orthogneiss; Chichorro *et al.* 2008), 526 ± 4 Ma (Barquete granite; Pereira *et al.* 2011), 525 ± 1 Ma (Barreiros granitic rock; Sánchez-García *et al.* 2014), 521 ± 10 Ma (Pavia orthogneiss; Dias da Silva *et al.* 2018), 522 ± 5 Ma and 517 ± 6 Ma (Escoural orthogneisses; Chichorro *et al.* 2008) and 518 ± 15 Ma (Pallares granodiorite; Ordóñez-Casado 1998).

Similarly, the protolith age obtained for the Valongo orthogneiss (496 ± 3 Ma; this study) is a more reliable indicator of Late Miaolingian–Early Furongian magmatic activity in the OMZ, which has been considered less representative than Terreneuvian activity. So far, OMZ igneous rocks with Furongian age include only rhyolites of the Estremoz volcano-sedimentary complex dated at 499 ± 3 Ma (Pereira *et al.* 2012*c*) and the Elvas syenites dated at 490 ± 4 Ma (Díez Fernández *et al.* 2015). This Upper Cambrian magmatism seems to have been associated with the extension of the North Gondwana margin in the aftermath of the Terreneuvian arc-rift transition, which continued later in the Ordovician (Sánchez-García *et al.* 2003; Díez Fernández *et al.* 2015; Solís-Alulima *et al.* 2020). In addition, zircon rims (i.e. overgrowths) in the age range from *c.* 488 Ma (Furongian; Almadén de la Plata amphibolite; Sánchez-Lorda *et al.* 2016) to *c.* 478 Ma (Tremadocian; granitic leucosome of the Cabril–Peña Grajera gneiss; Solís-Alulima *et al.* 2020) are reported in the OMZ, providing evidence for Furongian–Tremadocian magmatism and crustal partial melting of the North Gondwana margin.

Furthermore, new zircon U–Pb geochronology data provide evidence that the Cadomian crust was recycled in the OMZ during the Cambrian. Older zircon ages in the Terreneuvian Chancelaria orthogneiss match previous results reported for the inherited Neoproterozoic component found in OMZ igneous rocks of a similar age. The Terreneuvian Barquete granite and Cambrian-Series 2 Pallares granite, both emplaced in the Ediacaran Serie Negra Group that represents the oldest rocks of the OMZ (Eguíluz *et al.* 2000; Pereira *et al.* 2006), contain inherited Neoproterozoic zircon grains that are interpreted as being derived from the recycling of the Cadomian OMZ basement by partial melting (Pereira *et al.* 2011).

The same is true for the component of Neoproterozoic zircon grains in OMZ igneous rocks from two Cambrian magmatic pulses that preceded and followed the crystallization of Valongo igneous rock: Miaolingian (*c.* 509–505 Ma; Freixo-Segóvia rhyolite; Pereira *et al.* 2019, 2023*b*) and Tremadocian (Cabril–Peña Grajera gneiss; Solís-Alulima *et al.* 2020). Neoproterozoic inherited zircon ages closely resemble the age spectrum of detrital zircon from the Ediacaran and Terreneuvian metasedimentary rocks of the OMZ (Pereira *et al.* 2012*b*), indicating a crustal source that provided recycling of the Cadomian basement.

The oldest zircon grains (*c.* 587–508 Ma) found in the Furongian Valongo orthogneiss also suggest crustal reworking but, in this case, the inherited Neoproterozoic–Cambrian component was probably derived from sources with a wider age range, which may include Ediacaran to Miaolingian igneous rocks and/or sedimentary rocks.

To sum up, the time frame established for metamorphic processes suggests a close link between crustal recycling by partial melting and magmatism in the tectonic evolution of the OMZ from Terreneuvian to Furongian, which then continued in the Ordovician, and after a long break of more than 90 million years, in the Mississippian (Variscan orogeny).

Conclusions

New field mapping and petrographic studies enable the recognition of a D_2–M_2 tectono-thermal structure in the westernmost domains of the OMZ (i.e. the PSGD).

The PSGD is partially covered by the Cenozoic Tagus basin sedimentary rocks while showing a characteristic spatial distribution of telescoped metamorphic isograds that has never previously been adequately interpreted within the framework of the Mississippian synorogenic extension.

The gneiss dome features an infrastructure composed of the LGU and the ISU with Ediacaran–Cambrian sedimentary and igneous rocks deformed under the highest-grade M_2 metamorphic conditions that this OMZ region experienced (amphibolitic facies). Late Ediacaran–Early Terreneuvian and Late Miaolingian–Early Furongian protolith ages for the LGU (496 ± 3 Ma) and the ISU (539 ± 2 Ma) orthogneisses are reported based on new U–Pb SHRIMP zircon dating. The LGU and the ISU are separated by early D_2 ductile extensional shear zones. The USU Cambrian–Devonian sedimentary and igneous rocks that were deformed under M_2 lowest-grade metamorphic conditions (greenschist facies) constitute the superstructure. The USU is tectonically juxtaposed against the ISU by an early

D_2 ductile extensional shear zone. The USU was mainly deformed by pure shearing and compressed vertically, but locally simple shearing developed along discrete and conjugated D_2 extensional shear zones. Kinematic criteria associated with the main D_2–M_2 fabric indicate top-to-ESE–SE sense of shear.

A late-D_2 brittle-ductile high-angle extensional shear zone (i.e. Seda shear zone) crosscuts the dome structure, increasing the metamorphic difference between the infrastructure and the superstructure. The most recent Variscan D_3 contractional deformation event led to the development of D_3 upright folds, thrusts and transpressive shear zones that caused the steepening of earlier D_2 structures and the local crenulation of S_2 foliation.

The Mississippian D_2–M_2 event, which is well developed in the OMZ, may be regarded as a phenomenon at the regional scale that markedly influenced the crustal architecture of North Gondwana.

Acknowledgements This work is a contribution to IDL Research Group 3 (Solid Earth Dynamics, Hazards and Resources) and project grant No PID2020-117332GB-C21 (Spanish Agency of Science and Technology). We are grateful for detailed comments from Carlos Fernández and Olivier Vanderhaeghe that have contributed decisively to improve the content of this manuscript. We also acknowledge to Stacy Scott for the final editorial work and pagination, and to the editor Damian Nance by the final gramatical and orthographic polish of the preprint version of this manuscript. Last, but not least, we thank Sofia Rodrigues (thin-section laboratory technician of IDL-FCUL) for her dedication in the preparation of our samples.

Competing interests The authors declare that they have no known competing financial interests or personal relationships that could have appeared to influence the work reported in this paper.

Author contributions **ÍDDS**: conceptualization (equal), data curation (lead), investigation (lead), methodology (equal), writing – original draft (equal), writing – review & editing (equal); **MFP**: conceptualization (lead), investigation (equal), methodology (equal), supervision (lead), writing – original draft (lead), writing – review & editing (equal); **CG**: data curation (equal), investigation (supporting), methodology (supporting), validation (equal), writing – original draft (supporting); **LSH**: data curation (supporting), investigation (supporting), methodology (supporting); **SBS**: data curation (equal), formal analysis (equal), methodology (equal), validation (supporting), writing – original draft (supporting); **KDSA**: data curation (equal), formal analysis (supporting), investigation (supporting), methodology (supporting), writing – original draft (supporting); **JGB**: funding acquisition (equal), methodology (supporting), project administration (lead), writing – original draft (supporting); **CCGT**: methodology (equal), resources (lead), validation (equal), writing – original draft (supporting); **KS**: data curation (equal), methodology (equal), resources (equal), writing – original draft (supporting).

Funding This project was funded by MCIN/AEI/10.13039/501100011033 (Grant PID2020-117332GB-C21) and TED2021-130440B-I00. Í. Dias da Silva acknowledges financial support from the Portuguese Foundation for Science and Technology and I.P./MCTES (grants: FCT/UID/GEO/50019/2019-IDL and FCT/UIDB/ 50019/2020-IDL) and his national science contract in the FCUL funded by FCT 'Estímulo ao Emprego Científico-Norma Transitória'. M.F. Pereira and C. Gama acknowledge financial support from the Fundação para a Ciência e Tecnologia (Portuguese Foundation for Science and Technology) project (grant No FCT/UIDB/04683/2020-ICT).

Data availability All data generated or analysed during this study are included in this published article and its supplementary information files.

References

Abalos, B., Gil Ibarguchi, J.I. and Eguiluz, L. 1991. Cadomian subduction/collision and Variscan transpression in the Badajoz-Córdoba shear belt, southwest Spain. *Tectonophysics*, **199**, 51–72, https://doi.org/10.1016/0040-1951(91)90118-C

Abati, J., Gerdes, A., Fernández Suárez, J., Arenas, R., Whitehouse, M.J. and Díez Fernández, R. 2010. Magmatism and early-Variscan continental subduction in the northern Gondwana margin recorded in zircons from the basal units of Galicia, NW Spain. *Geological Society of America Bulletin*, **122**, 219–235, https://doi.org/10.1130/b26572.1

Abati, J., Arenas, R., Díez Fernández, R., Albert, R. and Gerdes, A. 2018. Combined zircon U-Pb and Lu-Hf isotopes study of magmatism and high-P metamorphism of the basal allochthonous units in the SW Iberian Massif (Ossa-Morena complex). *Lithos*, **322**, 20–37, https://doi.org/10.1016/j.lithos.2018.07.032

Alcock, J.E., Martínez Catalán, J.R. *et al*. 2015. 2-D thermal modeling of HT-LP metamorphism in NW and Central Iberia: implications for Variscan magmatism, rheology of the lithosphere and orogenic evolution. *Tectonophysics*, **657**, 21–37, https://doi.org/10.1016/j.tecto.2015.05.022

Antunes, A., Santos, J., Azevedo, M. and Corfu, F. 2011. New U-Pb zircon age constraints for the emplacement of the Reguengos de Monsaraz Massif (Ossa Morena Zone). *In*: Molina, J.F., Scarrow, J.H., Bea, F. and Montero, P. (eds) *Seventh Hutton Symposium on Granites and Related Rocks*. Universidad de Salamanca, Ávila, 9–10.

Apalategui, O., Eguiluz, L. and Quesada, C. 1990. Ossa Morena Zone, Structure. *In*: Dallmeyer, R.D. and Martínez García, E. (eds) *Pre-Mesozoic Geology of Iberia*. Springer, Berlin, 80–219.

Apraiz, A. and Eguíluz, L. 2002. Hercynian tectonothermal evolution associated with crustal extension and exhumation of the Lora del Río metamorphic

core complex (Ossa-Morena zone, Iberian Massif, SW Spain). *International Journal of Earth Sciences*, **91**, 76–92, https://doi.org/10.1007/s005310100206

Arenas, R., Ibarguchi, J.G., González Lodeiro, F., Klein, E. and Martínez Catalán, J.R. 1986. Tectonostratigraphic units in the complexes with mafic and related rocks of the NW of the Iberian Massif. *Hercynica*, **2**, 87–110.

Arenas, R., Díez Fernández, R., Sánchez Martínez, S., Gerdes, A., Fernández-Suárez, J. and Albert, R. 2014. Two-stage collision: exploring the birth of Pangea in the Variscan terranes. *Gondwana Research*, **25**, 756–763, https://doi.org/10.1016/j.gr.2013.08.009

Arenas, R., Novo-Fernández, I. *et al*. 2021. A unique blueschist facies metapelite with Mg-rich chloritoid from the Badajoz-Córdoba Unit (SW Iberian Massif): correlation of Late Devonian high-pressure belts along the Variscan Orogen. *International Geology Review*, **63**, 1634–1657, https://doi.org/10.1080/00206814.2020.1789509

Azor, A., Lodeiro, F.G. and Simancas, J.F. 1994. Tectonic evolution of the boundary between the Central Iberian and Ossa-Morena zones (Variscan belt, southwest Spain). *Tectonics*, **13**, 45–61, https://doi.org/10.1029/93TC02724

Azor, A., Rubatto, D., Simancas, J.F., González Lodeiro, F., Martínez Poyatos, D., Martín Parra, L.M. and Matas, J. 2008. Rheic Ocean ophiolitic remnants in southern Iberia questioned by SHRIMP U-Pb zircon ages on the Beja-Acebuches amphibolites. *Tectonics*, **27**, TC5006, https://doi.org/10.1029/2008TC002306

Barbero, L., Villaseca, C., Rogers, G. and Brown, P.E. 1995. Geochemical and isotopic disequilibrium in crustal melting: an insight from the anatectic granitoids from Toledo, Spain. *Journal of Geophysical Research: Solid Earth*, **100**, 15745–15765, https://doi.org/10.1029/95JB00036

Black, L.P., Kamo, S.L., Allen, C.M., Aleinikoff, J.N., Davis, D.W., Korsch, R.J. and Foudoulis, C. 2003. TEMORA 1: a new zircon standard for Phanerozoic U-Pb geochronology. *Chemical Geology*, **200**, 155–170, https://doi.org/10.1016/S0009-2541(03)00165-7

Brun, J.-P. and Faccenna, C. 2008. Exhumation of high-pressure rocks driven by slab rollback. *Earth and Planetary Science Letters*, **272**, 1–7, https://doi.org/10.1016/j.epsl.2008.02.038

Brun, J.P. and Van der Driessche, J. 1994. Extensional gneiss domes and detachment faults-structure and kinematics. *Bulletin de la Société Géologique de France*, **165**, 519–530.

Burg, J.P., Kaus, B.J.P. and Podladchikov, Y.Y. 2004. Dome structures in collision orogens: mechanical investigation of the gravity/compression interplay. *In*: Whitney, D.L., Teyssier, C. and Siddoway, C.S. (eds) *Gneiss Domes in Orogeny*. Geological Society of America, Boulder, CO, 47–66, https://doi.org/10.1130/0-8137-2380-9.47

Cambeses, A., Scarrow, J.H., Montero, P., Molina, J.F. and Moreno, J.A. 2015. SHRIMP U–Pb zircon dating of the Valencia del Ventoso plutonic complex, Ossa-Morena Zone, SW Iberia: early Carboniferous intra-orogenic extension-related 'calc-alkaline' magmatism. *Gondwana Research*, **28**, 735–756, https://doi.org/10.1016/j.gr.2014.05.013

Cawood, P.A., Kröner, A., Collins, W.J., Kusky, T.M., Mooney, W.D. and Windley, B.F. 2009. Accretionary orogens through Earth history. *Geological Society, London, Special Publications*, **318**, 1–36, https://doi.org/10.1144/SP318.1

Chichorro, M., Pereira, M.F., Díaz-Azpiroz, M., Williams, I.S., Fernández, C., Pin, C. and Silva, J.B. 2008. Cambrian ensialic rift-related magmatism in the Ossa-Morena Zone (Évora-Aracena metamorphic belt, SW Iberian Massif): Sm-Nd isotopes and SHRIMP zircon U-Th-Pb geochronology. *Tectonophysics*, **461**, 91–113, https://doi.org/10.1016/j.tecto.2008.01.008

Collins, W.J. 2002. Hot orogens, tectonic switching, and creation of continental crust. *Geology*, **30**, 535–538, https://doi.org/10.1130/0091-7613(2002)030<0535:HOTSAC>2.0.CO;2

Coney, P.J. 1980. Cordilleran metamorphic core complexes: an overview. *Geological Society of America Memoirs*, **153**, 7–31, https://doi.org/10.1130/MEM153-p7

Costa, S. and Rey, P. 1995. Lower crustal rejuvenation and growth during post-thickening collapse: insights from a crustal cross section through a Variscan metamorphic core complex. *Geology*, **23**, 905–908, https://doi.org/10.1130/0091-7613(1995)023<0905:lcragd>2.3.co;2

Denèle, Y., Olivier, P., Gleizes, G. and Barbey, P. 2007. The Hospitalet gneiss dome (Pyrenees) revisited: lateral flow during Variscan transpression in the middle crust. *Terra Nova*, **19**, 445–453, https://doi.org/10.1111/j.1365-3121.2007.00770.x

Dewey, J.F. 1988. Extensional collapse of orogens. *Tectonics*, **7**, 1123–1139, https://doi.org/10.1029/TC007i006p01123

Dias da Silva, Í. 2014. *Geología de las Zonas Centro Ibérica y Galicia – Trás-os-Montes en la parte oriental del Complejo de Morais, Portugal/España*. Instituto Universitario de Geología "Isidro Parga Pondal" - Área de Xeoloxía e Minería do Seminario de Estudos Galegos, Coruña.

Dias da Silva, Í., Gómez-Barreiro, J., Martínez Catalán, J.R., Ayarza, P., Pohl, J. and Martínez, E. 2017. Structural and microstructural analysis of the Retortillo Syncline (Variscan belt, Central Iberia). Implications for the Central Iberian Orocline. *Tectonophysics*, **717**, 99–115, https://doi.org/10.1016/j.tecto.2017.07.015

Dias da Silva, Í., Pereira, M.F., Silva, J.B. and Gama, C. 2018. Time-space distribution of silicic plutonism in a gneiss dome of the Iberian Variscan Belt: the Évora Massif (Ossa-Morena Zone, Portugal). *Tectonophysics*, **747–748**, 298–317, https://doi.org/10.1016/j.tecto.2018.10.015

Dias da Silva, Í., González Clavijo, E. and Díez-Montes, A. 2021. The collapse of the Variscan belt: a Variscan lateral extrusion thin-skinned structure in NW Iberia. *International Geology Review*, **63**, 659–695, https://doi.org/10.1080/00206814.2020.1719544

Díaz-Alvarado, J., Fernández, C., Díaz-Azpiroz, M., Castro, A. and Moreno-Ventas, I. 2012. Fabric evidence for granodiorite emplacement with extensional shear zones in the Variscan Gredos massif (Spanish Central System). *Journal of Structural Geology*, **42**, 74–90, https://doi.org/10.1016/j.jsg.2012.06.012

Díez Balda, M.A., Martínez Catalán, J.R. and Ayarza Arribas, P. 1995. Syn collisional extensional collapse parallel to orogenic trend in a domain of steep tectonics: the Salamanca Detachment Zone (Central Iberian Zone, Spain). *Journal of Structural Geology*, **17**, 163–182, https://doi.org/10.1016/0191-8141(94)E0042-W

Díez Fernández, R. and Arenas, R. 2015. The Late Devonian Variscan suture of the Iberian Massif: a correlation of high-pressure belts in NW and SW Iberia. *Tectonophysics*, **654**, 96–100, https://doi.org/10.1016/j.tecto.2015.05.001

Díez Fernández, R. and Pereira, M.F. 2016. Extensional orogenic collapse captured by strike-slip tectonics: constraints from structural geology and UPb geochronology of the Pinhel shear zone (Variscan orogen, Iberian Massif). *Tectonophysics*, **691**, 290–310, https://doi.org/10.1016/j.tecto.2016.10.023

Díez Fernández, R., Martínez Catalán, J.R., Gerdes, A., Abati, J., Arenas, R. and Fernández-Suárez, J. 2010. U-Pb ages of detrital zircons from the Basal allochthonous units of NW Iberia: provenance and paleoposition on the northern margin of Gondwana during the Neoproterozoic and Paleozoic. *Gondwana Research*, **18**, 385–399, https://doi.org/10.1016/j.gr.2009.12.006

Díez Fernández, R., Martínez Catalán, J.R., Gómez Barreiro, J. and Arenas, R. 2012. Extensional flow during gravitational collapse: a tool for setting plate convergence (Padrón migmatitic dome, Variscan belt, NW Iberia). *Journal of Geology*, **120**, 83–103, https://doi.org/10.1086/662735

Díez Fernández, R., Pereira, M.F. and Foster, D.A. 2015. Peralkaline and alkaline magmatism of the Ossa-Morena zone (SW Iberia): age, source, and implications for the Paleozoic evolution of Gondwanan lithosphere. *Lithosphere*, **7**, 73–90, https://doi.org/10.1130/l379.1

Díez Fernández, R., Arenas, R. *et al*. 2016. Tectonic evolution of Variscan Iberia: Gondwana–Laurussia collision revisited. *Earth-Science Reviews*, **162**, 269–292, https://doi.org/10.1016/j.earscirev.2016.08.002

Díez Fernández, R., Fuenlabrada, J.M., Chichorro, M., Pereira, M.F., Sánchez-Martínez, S., Silva, J.B. and Arenas, R. 2017. Geochemistry and tectonostratigraphy of the basal allochthonous units of SW Iberia (Évora Massif, Portugal): keys to the reconstruction of pre-Pangean paleogeography in southern Europe. *Lithos*, **268–271**, 285–301, https://doi.org/10.1016/j.lithos.2016.10.031

Díez Fernández, R., Fernández, C., Arenas, R. and Novo-Fernández, I. 2021. On the rootless nature of a Devonian suture in SW Iberia (Ossa-Morena Complex, Variscan Orogen): geometry and kinematics of the Azuaga Fault. *Tectonics*, **40**, https://doi.org/10.1029/2021TC006791

Eguíluz, L., Ibarguchi, J.I.G., Ábalos, B. and Apraiz, A. 2000. Superposed Hercynian and Cadomian orogenic cycles in the Ossa-Morena zone and related areas of the Iberian Massif. *GSA Bulletin*, **112**, 1398–1413, https://doi.org/10.1130/0016-7606(2000)112<1398:shacoc>2.0.co;2

Escuder Viruete, J., Arenas, R. and Martínez Catalán, J.R. 1994. Tectonothermal evolution associated with Variscan crustal extension, in the Tormes Gneiss dome (NW Salamanca, Iberian Massif, Spain). *Tectonophysics*, **238**, 1–22, https://doi.org/10.1016/0040-1951(94)90052-3

Faure, M., Lardeaux, J.-M. and Ledru, P. 2009. A review of the pre-Permian geology of the Variscan French Massif Central. *Comptes Rendus Geoscience*, **341**, 202–213, https://doi.org/10.1016/j.crte.2008.12.001

Ferreira, P. and Piçarra, J.M. 2020. *Folha 6 da Carta Geológica de Portugal à escala 1:200.000*. LNEG.

Franke, W. 2000. The mid-European segment of the Variscides: tectonostratigraphic units, terrane boundaries and plate tectonic evolution. *Geological Society, London, Special Publications*, **179**, 35–61, https://doi.org/10.1144/gsl.sp.2000.179.01.05

Franke, W. 2014. Topography of the Variscan orogen in Europe: failed–not collapsed. *International Journal of Earth Sciences*, **103**, 1471–1499, https://doi.org/10.1007/s00531-014-1014-9

Galopim de Carvalho, A.M., Zbyszewsky, G., Carvalhosa, A. and Veiga Ferreira, O. 1981. *Carta Geológica de Portugal na escala 1:50.000, Folha 32-A (Ponte de Sor)*.

Gapais, D., Brun, J.-P., Gumiaux, C., Cagnard, F., Ruffet, G. and Le Carlier De Veslud, C. 2015. Extensional tectonics in the Hercynian Armorican belt (France): an overview. *Bulletin de la Société Géologique de France*, **186**, 117–129, https://doi.org/10.2113/gssgfbull.186.2-3.117

Gómez Barreiro, J., Martínez Catalán, J.R., Arenas, R., Castiñeiras, P., Abati, J., Díaz García, F. and Wijbrans, J.R. 2007. Tectonic evolution of the upper allochtonon of the Órdenes complex (Northwestern Iberian Massif): structural constraints to a poligenic peri-Gondwanan terrane. *Geologic Society of America, Special Paper*, **423**, 315–332, https://doi.org/10.1130/2007.2423(15)

Gonçalves, F. 1973. *Carta Geológica de Portugal na escala 1:50.000, Folha 32-B (Portalegre)*.

González Clavijo, E., Dias da Silva, Í. *et al*. 2021. A tectonic carpet of Variscan flysch at the base of a rootless accretionary prism in northwestern Iberia: U–Pb zircon age constrains from sediments and volcanic olistoliths. *Solid Earth*, **12**, 835–867, https://doi.org/10.5194/se-12-835-2021

Gray, R. and Pysklywec, R.N. 2012. Geodynamic models of mature continental collision: evolution of an orogen from lithospheric subduction to continental retreat/delamination. *Journal of Geophysical Research: Solid Earth*, **117**, B03408, https://doi.org/10.1029/2011JB008692

Gutiérrez-Alonso, G., Fernández-Suárez, J., López-Carmona, A. and Gärtner, A. 2018. Exhuming a cold case: the early granodiorites of the northwest Iberian Variscan belt–a Visean magmatic flare-up? *Lithosphere*, **10**, 194–216, https://doi.org/10.1130/L706.1

Gutiérrez-Marco, J.C. and Robardet, M. 2004. The Ordovician, Silurian and Devonian sedimentary rocks of the Ossa-Morena Zone (SW Iberian Peninsula, Spain). *Journal of Iberian Geology*, **30**, 73–92.

Hanchar, J.M. and Miller, C.F. 1993. Zircon zonation patterns as revealed by cathodoluminescence and back-scattered electron images: implications for interpretation of complex crustal histories. *Chemical Geology*, **110**, 1–13, https://doi.org/10.1016/0009-2541(93)90244-D

Heaman, L.M., Bowins, R. and Crocket, J. 1990. The chemical composition of igneous zircon suites:

implications for geochemical tracer studies. *Geochimica et Cosmochimica Acta*, **54**, 1597–1607, https://doi.org/10.1016/0016-7037(90)90394-Z

Hoskin, P.W.O. and Schaltegger, U. 2003. The composition of zircon and igneous and metamorphic petrogenesis. *Reviews in Mineralogy and Geochemistry*, **53**, 27–62, https://doi.org/10.2113/0530027

Jolivet, L. and Brun, J.-P. 2010. Cenozoic geodynamic evolution of the Aegean. *International Journal of Earth Sciences*, **99**, 109–138, https://doi.org/10.1007/s00531-008-0366-4

Lima, S.M., Corfu, F., Neiva, A.M.R. and Ramos, J.M.F. 2012. Dissecting complex magmatic processes: an in-depth U–Pb Study of the Pavia Pluton, Ossa–Morena Zone, Portugal. *Journal of Petrology*, **53**, 1887–1911, https://doi.org/10.1093/petrology/egs037

Linnemann, U., Pereira, M.F., Jeffries, T.E., Drost, K. and Gerdes, A. 2008. The Cadomian Orogeny and the opening of the Rheic Ocean: the diachrony of geotectonic processes constrained by LA-ICP-MS U-Pb zircon dating (Ossa-Morena and Saxo-Thuringian Zones, Iberian and Bohemian Massifs). *Tectonophysics*, **461**, 21–43, https://doi.org/10.1016/j.tecto.2008.05.002

Lister, G.S., Banga, G. and Feenstra, A. 1984. Metamorphic core complexes of Cordilleran type in the Cyclades, Aegean Sea, Greece. *Geology*, **12**, 221–225, https://doi.org/10.1130/0091-7613(1984)12<221:mccoct>2.0.co;2

López-Carmona, A., Abati, J., Pitra, P. and Lee, J.W. 2014. Retrogressed lawsonite blueschists from the NW Iberian Massif: P–T–t constraints from thermodynamic modelling and 40Ar/39Ar geochronology. *Contributions to Mineralogy and Petrology*, **167**, 1–20, https://doi.org/10.1007/s00410-014-0987-5

López-Moro, F.J., López-Plaza, M., Gutiérrez-Alonso, G., Fernández-Suárez, J., López-Carmona, A., Hofmann, M. and Romer, R.L. 2018. Crustal melting and recycling: geochronology and sources of Variscan syn-kinematic anatectic granitoids of the Tormes Dome (Central Iberian Zone). A U-Pb LA-ICP-MS study. *International Journal of Earth Sciences*, **107**, 985–1004, https://doi.org/10.1007/s00531-017-1483-8

Ludwig, K.R. 2003. *Isoplot 3.00: A Geochronological Toolkit for Microsoft Excel© (Revised Version)*. Berkeley Geochronological Center, Special Publication, **4**.

Martins, F., Azevedo, M.R., Valle Aguado, B., Gomes, E.P., Tassinari, C. and Nogueira Neto, J. 2021. SHRIMP U-Pb ages and REE patterns for zircon from an anatectic Variscan two-mica granite from the Bemposta Migmatite Complex (Central Iberian Zone). *The Canadian Mineralogist*, **58**, 847–861, https://doi.org/10.3749/canmin.2000015

Martínez Catalán, J.R. 2011. Are the oroclines of the Variscan belt related to late Variscan strike-slip tectonics? *Terra Nova*, **23**, 241–247, https://doi.org/10.1111/j.1365-3121.2011.01005.x

Martínez Catalán, J.R., Arenas, R. and Díez Balda, M.A. 2003. Large extensional structures developed during the emplacement of a crystalline thrust sheet: the Mondoñedo nappe (NW Spain). *Journal of Structural Geology*, **25**, 1815–1839, https://doi.org/10.1016/S0191-8141(03)00038-5

Martínez Catalán, J.R., Arenas, R. *et al*. 2007. Space and time in the tectonic evolution of the northwestern Iberian Massif: Implications for the Variscan belt. *In*: Hatcher, R.D., , Jr, Carlson, M.P., McBride, J.H. and Martínez Catalán, J.R. (eds) *4-D Framework of Continental Crust*. Geological Society of America, Boulder, CO, 403–423, https://doi.org/10.1130/2007.1200(21)

Martínez Catalán, J.R., Arenas, R. *et al*. 2009. A rootless suture and the loss of the roots of a mountain chain: the Variscan Belt of NW Iberia. *CR Geoscience*, **341**, 114–126, https://doi.org/10.1016/j.crte.2008.11.004

Martínez Catalán, J.R., Schulmann, K. and Ghienne, J.-F. 2021. The Mid-Variscan Allochthon: keys from correlation, partial retrodeformation and plate-tectonic reconstruction to unlock the geometry of a non-cylindrical belt. *Earth-Science Reviews*, **220**, 103700, https://doi.org/10.1016/j.earscirev.2021.103700

Matte, P. 2001. The Variscan collage and orogeny (480–290 Ma) and the tectonic definition of the Armorica microplate: a review. *Terra Nova*, **13**, 122–128, https://doi.org/10.1046/j.1365-3121.2001.00327.x

Matte, P. 2007. Variscan thrust nappes, detachments, and strike-slip faults in the French Massif Central: interpretation of lineations. *In*: Hatcher, R.D., Jr, Carlson, M.P., McBride, J.H. and Martínez Catalán, J.R. (eds) *4D Framework of Continental Crust*. Geological Society of America, Boulder, CO, 391–402, https://doi.org/10.1130/2007.1200(20)

Moita, P., Munhá, J., Fonseca, P.E., Pedro, J., Tassinari, C.C.G., Araújo, A. and Palácios, T. 2005. Phase equilibria and geochronology of Ossa-Morena eclogites. *XIV Semana de Geoquímica – VIII Congresso de Geoquímica dos Países de Língua Portuguesa*. Universidade de Aveiro, Aveiro, 463–466.

Moita, P., Santos, J.F., Pereira, M.F., Costa, M.M. and Corfu, F. 2015. The quartz-dioritic Hospitais intrusion (SW Iberian Massif) and its mafic microgranular enclaves-evidence for mineral clustering. *Lithos*, **224–225**, 78–100, https://doi.org/10.1016/j.lithos.2015.02.012

Montero, P., Salman, K. *et al*. 2000. New data on the geochronology of the Ossa-Morena Zone, Iberian Massif. *Basement Tectonics*, **15**, 136–138.

Moreno-Martín, D., Díez Fernández, R., de Vicente, G., Fernández, C. and Gómez Barreiro, J. 2022. Orogenic reworking and reactivation in Central Iberia: a record of Variscan, Permian and Alpine tectonics. *Tectonophysics*, **843**, 229601, https://doi.org/10.1016/j.tecto.2022.229601

Murphy, J.B. and Nance, R.D. 2013. Speculations on the mechanisms for the formation and breakup of supercontinents. *Geoscience Frontiers*, **4**, 185–194, https://doi.org/10.1016/j.gsf.2012.07.005

Novo-Fernández, I., Arenas, R., de Capitani, C., Pereira, M.F., Díez Fernández, R., Sánchez Martínez, S. and Garcia-Casco, A. 2021. Tracking the Late Devonian high-P metamorphic belt in the Variscan Orogen: new constraints on the PT evolution of eclogites from the Cubito-Moura Unit (SW Iberian Massif). *Lithos*, **386–387**, 106015, https://doi.org/10.1016/j.lithos.2021.106015

Ordóñez-Casado, B. 1998. *Geochronological studies of the pre-Mesozoic basement of the Iberian Massif: the Ossa*

Morena zone and the Allochthonous Complexes within the Central Iberian zone. PhD thesis, ETH.

Passchier, C.W. and Trouw, R.A.J. 2005. *Microtectonics*, 2nd edn. Springer, Berlin.

Pastor-Galán, D., Dias da Silva, Í., Groenewegen, T. and Krijgsman, W. 2019. Tangled up in folds: tectonic significance of superimposed folding at the core of the Central Iberian curve (West Iberia). *International Geology Review*, **61**, 240–255, https://doi.org/10.1080/00206814.2017.1422443

Pereira, M.F., Chichorro, M., Linnemann, U., Eguiluz, L. and Silva, J.B. 2006. Inherited arc signature in Ediacaran and Early Cambrian basins of the Ossa-Morena Zone (Iberian Massif, Portugal): paleogeographic link with European and North African Cadomian correlatives. *Precambrian Research*, **144**, 297–315, https://doi.org/10.1016/j.precamres.2005.11.011

Pereira, M.F., Silva, J.B., Chichorro, M., Moita, P.C., Santos, J.F., Apraiz, A. and Ribeiro, C. 2007. Crustal growth and deformational processes in the northern Gondwana margin: constraints from the Évora Massif (Ossa-Morena zone, southwest Iberia, Portugal) *In*: Linnemann, U., Nance, R.D., Kraft, P. and Zulauf, G. (eds) *The Evolution of the Rheic Ocean: From Avalonian-Cadomian Active Margin to Alleghenian-Variscan Collision*. Geological Society of America, https://doi.org/10.1130/2007.2423(16)

Pereira, M.F., Chichorro, M. *et al*. 2009. Variscan intra-orogenic extensional tectonics in the Ossa-Morena Zone (Évora-Aracena-Lora del Río metamorphic belt, SW Iberian Massif): SHRIMP zircon U-Th-Pb geochronology. *Geological Society, London, Special Publications*, **327**, 215–237, https://doi.org/10.1144/sp327.11

Pereira, M.F., Apraiz, A., Chichorro, M., Silva, J.B. and Armstrong, R.A. 2010. Exhumation of high-pressure rocks in northern Gondwana during the Early Carboniferours (Coimbra-Cordoba shear zone, SW Iberian Massif): tectonothermal analysis and U-Pb SHRIMP in-situ zircon geochronology. *Gondwana Research*, **17**, 440–460, https://doi.org/10.1016/j.gr.2009.10.001

Pereira, M.F., Chichorro, M., Solá, A.R., Silva, J.B., Sánchez-García, T. and Bellido, F. 2011. Tracing the Cadomian magmatism with detrital/inherited zircon ages by in-situ U–Pb SHRIMP geochronology (Ossa-Morena Zone, SW Iberian Massif). *Lithos*, **123**, 204–217, https://doi.org/10.1016/j.lithos.2010.11.008

Pereira, M.F., Chichorro, M., Silva, J.B., Ordóñez-Casado, B., Lee, J.K.W. and Williams, I.S. 2012*a*. Early carboniferous wrenching, exhumation of high-grade metamorphic rocks and basin instability in SW Iberia: constraints derived from structural geology and U–Pb and 40Ar–39Ar geochronology. *Tectonophysics*, **558–559**, 28–44, https://doi.org/10.1016/j.tecto.2012.06.020

Pereira, M.F., Linnemann, U., Hofmann, M., Chichorro, M., Solá, A.R., Medina, J. and Silva, J.B. 2012*b*. The provenance of Late Ediacaran and Early Ordovician siliciclastic rocks in the Southwest Central Iberian Zone: constraints from detrital zircon data on northern Gondwana margin evolution during the late Neoproterozoic. *Precambrian Research*, **192–195**, 166–189, https://doi.org/10.1016/j.precamres.2011.10.019

Pereira, M.F., Solá, A.R., Chichorro, M., Lopes, L., Gerdes, A. and Silva, J.B. 2012*c*. North-Gondwana assembly, break-up and paleogeography: U/Pb isotope evidence from detrital and igneous zircons of Ediacaran and Cambrian rocks of SW Iberia. *Gondwana Research*, **22**, 866–881, https://doi.org/10.1016/j.gr.2012.02.010

Pereira, M.F., Castro, A. and Fernández, C. 2015. The inception of a Paleotethyan magmatic arc in Iberia. *Geoscience Frontiers*, **6**, 297–306, https://doi.org/10.1016/j.gsf.2014.02.006

Pereira, M.F., Gutíerrez-Alonso, G., Murphy, J.B., Drost, K., Gama, C. and Silva, J.B. 2017. Birth and demise of the Rheic Ocean magmatic arc(s): combined U–Pb and Hf isotope analyses in detrital zircon from SW Iberia siliciclastic strata. *Lithos*, **278**, 383–399, https://doi.org/10.1016/j.lithos.2017.02.009

Pereira, M., Dias da Silva, Í., Gama, C. and Silva, J.B. 2019. Revisiting the Ediacaran-Cambrian boundary in the Ossa-Morena Zone (SW Iberia). *In*: Alvaro, J.J. and Jensen, S. (eds) *International Meeting on the Ediacaran System and the Ediacaran-Cambrian Transition*. Consejo Superior de Investigaciones Científicas, Guadalupe, Spain, 31–32.

Pereira, M.F., Gama, C., Dias da Silva, Í., Fuenlabrada, J.M., Silva, J.B. and Medina, J. 2020*a*. Isotope geochemistry evidence for Laurussian-type sources of South Portuguese Zone Carboniferous turbidites (Variscan Orogeny). *Geological Society, London, Special Publications*, **503**, 619–642, https://doi.org/10.1144/sp503-2019-163

Pereira, M.F., Gama, C., Dias da Silva, Í., Silva, J.B., Hofmann, M., Linnemann, U. and Gärtner, A. 2020*b*. Chronostratigraphic framework and provenance of the Ossa-Morena Zone Carboniferous basins (southwest Iberia). *Solid Earth*, **11**, 1291–1312, https://doi.org/10.5194/se-11-1291-2020

Pereira, M.F., Fernández, C., Rodríguez, C. and Castro, A. 2022*a*. Ordovician tectonics and crustal evolution at the Gondwana margin (Central Iberian Zone). *Journal of the Geological Society, London*, **179**, https://doi.org/10.1144/jgs2021-168

Pereira, M.F., Fuenlabrada, J.M., Rodríguez, C. and Castro, A. 2022*b*. Changing Carboniferous Arc Magmatism in the Ossa-Morena Zone (Southwest Iberia): implications for the Variscan Belt. *Minerals*, **12**, 22, https://doi.org/10.3390/min12050597

Pereira, M.F., Dias da Silva, Í., Rodríguez, C., Corfu, F. and Castro, A. 2023*a*. Visean high-K mafic-intermediate plutonic rocks of the Ossa-Morena Zone (SW Iberia): implications for regional extensional tectonics. *Geological Society, London, Special Publications*, **531**, https://doi.org/10.1144/SP531-2022-11

Pereira, M.F., Gama, C., Dias da Silva, Í., Fuenlabrada, J.M. and El Houicha, M. 2023*b*. Cadomian arc recycling along the northern Gondwana margin: Source-inherited composition of Miaolingian rift-related rhyolitic rocks (Ossa-Morena Zone, SW Iberia). *Journal of African Earth Sciences*, **201**, 104887, https://doi.org/10.1016/j.jafrearsci.2023.104887

Pin, C., Fonseca, P.E., Paquette, J.-L., Castro, P. and Matte, P. 2008. The ca. 350 Ma Beja Igneous Complex: a record of transcurrent slab break-off in the Southern Iberia Variscan Belt? *Tectonophysics*, **461**, 356–377, https://doi.org/10.1016/j.tecto.2008.06.001

Platt, J.P., Behr, W.M. and Cooper, F.J. 2015. Metamorphic core complexes: windows into the mechanics and

rheology of the crust. *Journal of the Geological Society, London*, **172**, 9–27, https://doi.org/10.1144/jgs2014-036

Quesada, C. 1996. Evolución geodinámica de la Zona de Ossa-Morena durante el ciclo Cadomiense. *In*: Araujo, A. and Pereira, M.F. (eds) *Estudos sobre a geología da Zona de Ossa Morena (Maciço Ibérico)*. Univ. Évora, Évora, 205–230.

Quesada, C. and Dallmeyer, R.D. 1994. Tectonothermal evolution of the Badajoz-Cordóba shear zone (SW Iberia): characteristics and 40Ar/39Ar mineral age constraints. *Tectonophysics*, **231**, 195–213, https://doi.org/10.1016/0040-1951(94)90130-9

Quesada, C., Robardet, M. and Gabaldón, V. 1990. Synorogenic Phase (Upper Devonian-Carboniferous-Lower Permian). *In*: Dallmeyer, R.D. and Martínez García, E. (eds) *Pre-Mesozoic Geology of Iberia*. Springer, Berlin, 273–278.

Rey, P. 1993. Seismic and tectono-metamorphic characters of the lower continental crust in Phanerozoic areas: a consequence of post-thickening extension. *Tectonics*, **12**, 580–590, https://doi.org/10.1029/92TC01568

Rodríguez, J., Cosca, M.A., Gil Ibarguchi, J.I. and Dallmeyer, R.D. 2003. Strain partitioning and preservation of 40Ar/39Ar ages during Variscan exhumation of a subducted crust (Malpica–Tui complex, NW Spain). *Lithos*, **70**, 111–139, https://doi.org/10.1016/S0024-4937(03)00095-1

Rodríguez, C., Pereira, M.F., Castro, A., Gutiérrez-Alonso, G. and Fernández, C. 2022. Variscan intracrustal recycling by melting of Carboniferous arc-like igneous protoliths (Évora Massif, Iberian Variscan belt). *GSA Bulletin*, **134**, 1549–1570, https://doi.org/10.1130/b36111.1

Romeo, I., Lunar, R., Capote, R., Quesada, C., Dunning, G.R., Piña, R. and Ortega, L. 2006. U–Pb age constraints on Variscan magmatism and Ni–Cu–PGE metallogeny in the Ossa–Morena Zone (SW Iberia). *Journal of the Geological Society, London*, **163**, 837–846, https://doi.org/10.1144/0016-76492005-065

Rubenach, M.J. and Bell, T.H. 1988. Microstructural controls and the role of graphite in matrix/porphyroblast exchange during synkinematic andalusite growth in a granitoid aureole. *Journal of Metamorphic Geology*, **6**, 651–666, https://doi.org/10.1111/j.1525-1314.1988.tb00446.x

Rubio Pascual, F.J., López-Carmona, A. and Arenas, R. 2016. Thickening v. extension in the Variscan belt: P–T modelling in the Central Iberian autochthon. *Tectonophysics*, **681**, 144–158, https://doi.org/10.1016/j.tecto.2016.02.033

Rubio Pascual, F.J., Martín Parra, L.M. *et al*. 2022. Tectonics and geothermal gradients from subduction to collision in the NW Variscan Iberian Massif. *International Geology Review*, forthcoming, https://doi.org/10.1080/00206814.2022.2073569

Sánchez-García, T., Bellido, F. and Quesada, C. 2003. Geodynamic setting and geochemical signatures of Cambrian–Ordovician rift-related igneous rocks (Ossa-Morena Zone, SW Iberia). *Tectonophysics*, **365**, 233–255, https://doi.org/10.1016/S0040-1951(03)00024-6

Sánchez-García, T., Quesada, C., Bellido, F., Dunning, G.R. and González del Tánago, J. 2008. Two-step magma flooding of the upper crust during rifting: the Early Paleozoic of the Ossa Morena Zone (SW Iberia). *Tectonophysics*, **461**, 72–90, https://doi.org/10.1016/j.tecto.2008.03.006

Sánchez-García, T., Pereira, M.F. *et al*. 2014. Early Cambrian granitoids of North Gondwana margin in the transition from a convergent setting to intra-continental rifting (Ossa-Morena Zone, SW Iberia). *International Journal of Earth Sciences*, **103**, 1203–1218, https://doi.org/10.1007/s00531-013-0939-8

Sánchez-Lorda, M.E., Ábalos, B., García de Madinabeitia, S., Eguíluz, L., Gil Ibarguchi, J.I. and Paquette, J.L. 2016. Radiometric discrimination of pre-Variscan amphibolites in the Ediacaran Serie Negra (Ossa-Morena Zone, SW Iberia). *Tectonophysics*, **681**, 31–45, https://doi.org/10.1016/j.tecto.2015.09.020

Sarrionandia, F., Ábalos, B. *et al*. 2020. Ediacaran – earliest Cambrian arc-tholeiite and adakite associations of the Malcocinado Formation (Ossa-Morena Zone, SW Spain): Juvenile continental crust and deep crustal reworking in northern Gondwana. *Lithos*, **372–373**, 105683, https://doi.org/10.1016/j.lithos.2020.105683

Sato, K., Tassinari, C.C.G., Basei, M.A.S., Siga Júnior, O. and Onoe, A.T. 2014. Sensitive High Resolution Ion Microprobe (SHRIMP IIe/MC) of the Institute of Geosciences of the University of São Paulo, Brazil: method and first results. *Geologia USP Série Científica*, **14**, 3–18, https://doi.org/10.5327/z1519-874x20140003 0001

Schulmann, K., Edel, J.-B. *et al*. 2022. Tectonic evolution and global crustal architecture of the European Variscan belt constrained by geophysical data. *Earth-Science Reviews*, **234**, 104195, https://doi.org/10.1016/j.earscirev.2022.104195

Simancas, J.F., Martínez Poyatos, D., Expósito, I., Azor, A. and González Lodeiro, F. 2001. The structure of a major suture zone in the SW Iberian Massif: the Ossa-Morena/Central Iberian contact. *Tectonophysics*, **332**, 295–308, https://doi.org/10.1016/S0040-1951(00)00262-6

Simancas, J.F., Carbonell, R. *et al*. 2003. Crustal structure of the transpressional Variscan orogen of SW Iberia: SW Iberia deep seismic reflection profile (IBERSEIS). *Tectonics*, **22**, https://doi.org/10.1029/2002tc001479

Simancas, J.F., Azor, A. *et al*. 2009. Tectonic relationships of Southwest Iberia with the allochthons of Northwest Iberia and the Moroccan Variscides. *Comptes Rendus Geoscience*, **341**, 103–113, https://doi.org/10.1016/j.crte.2008.11.003

Solís-Alulima, B., López-Carmona, A. and Abati, J. 2020. Ordovician metamorphism and magmatism preserved in the Ossa Morena Complex: SHRIMP geochronology, geochemistry and SrNd isotopic signatures of the Sierra Albarrana Domain (SW Iberian Massif). *Lithos*, **374–375**, 105700, https://doi.org/10.1016/j.lithos.2020.105700

Spear, F.S. 1995. *Metamorphic Phase Equilibria and Pressure-Temperature-Time Paths*. 2nd edn. Mineralogical Society of America, Chelsea.

Teyssier, C. and Whitney, D.L. 2002. Gneiss domes and orogeny. *Geology*, **30**, 1139–1142, https://doi.org/10.1130/0091-7613(2002)030<1139:GDAO>2.0.CO;2

Tirel, C.L., Brun, J.-P., Burov, E., Whitney, D.L., Teyssier, C. and Siddoway, C.S. 2004. Thermomechanical modeling of extensional gneiss domes *Gneiss Domes in Orogeny*. *Geological Society of America Special Papers*, **380**, 67–78, https://doi.org/10.1130/0-8137-2380-9.67

Ueda, K., Gerya, T.V. and Burg, J.-P. 2012. Delamination in collisional orogens: thermomechanical modeling. *Journal of Geophysical Research: Solid Earth*, **117**, B08202, https://doi.org/10.1029/2012JB009144

Vanardois, J., Trap, P. *et al*. 2022. Flow of the partially molten crust in the Variscan foreland revealed by U-Pb dating of metamorphism, magmatism and deformation (Agly Massif, Eastern Pyrenees). *International Journal of Earth Sciences*, **111**, 2101–2128, https://doi.org/10.1007/s00531-022-02229-7

Vanderhaeghe, O. 2004. Structural development of the Naxos migmatite dome. *Geological Society of America Special Papers*, **380**, 211–227 https://doi.org/10.1130/0-8137-2380-9.211

Vanderhaeghe, O. 2009. Migmatites, granites and orogeny: flow modes of partially molten rocks and magmas associated with melt/solid segregation in orogenic belts. *Tectonophysics*, **477**, 119–134, https://doi.org/10.1016/j.tecto.2009.06.021

Vanderhaeghe, O. 2012. The thermal–mechanical evolution of crustal orogenic belts at convergent plate boundaries: a reappraisal of the orogenic cycle. *Journal of Geodynamics*, **56–57**, 124–145, https://doi.org/10.1016/j.jog.2011.10.004

Vanderhaeghe, O. and Duchêne, S. 2010. Crustal-scale mass transfer, geotherm and topography at convergent plate boundaries. *Terra Nova*, **22**, 315–323, https://doi.org/10.1111/j.1365-3121.2010.00952.x

Vanderhaeghe, O., Burg, J.-P. and Teyssier, C. 1999*a*. Exhumation of migmatites in two collapsed orogens: Canadian Cordillera and French Variscides. *Geological Society, London, Special Publications*, **154**, 181–204, https://doi.org/10.1144/gsl.sp.1999.154.01.08

Vanderhaeghe, O., Teyssier, C. and Wysoczanski, R. 1999*b*. Structural and geochronological constraints on the role of partial melting during the formation of the Shuswap metamorphic core complex at the latitude of the Thor-Odin dome, British Columbia. *Canadian Journal of Earth Sciences*, **36**, 917–943, https://doi.org/10.1139/e99-023

Vanderhaeghe, O., Medvedev, S., Fullsack, P., Beaumont, C. and Jamieson, R.A. 2003. Evolution of orogenic wedges and continental plateaux: insights from crustal thermal-mechanical models overlying subducting mantle lithosphere. *Geophysical Journal International*, **153**, 27–51, https://doi.org/10.1046/j.1365-246X.2003.01861.x

Vanderhaeghe, O., Laurent, O. *et al*. 2020. Flow of partially molten crust controlling construction, growth and collapse of the Variscan orogenic belt: the geologic record of the French Massif Central. *BSGF – Earth Sciences Bulletin*, **191**, 56, https://doi.org/10.1051/bsgf/2020013

von Blanckenburg, F. and Davies, J.H. 1995. Slab breakoff: A model for syncollisional magmatism and tectonics in the Alps. *Tectonics*, **14**, 120–131, https://doi.org/10.1029/94TC02051

Wells, M.L. and Hoisch, T.D. 2008. The role of mantle delamination in widespread Late Cretaceous extension and magmatism in the Cordilleran orogen, western United States. *GSA Bulletin*, **120**, 515–530, https://doi.org/10.1130/b26006.1

Wernicke, B. 1981. Low-angle normal faults in the Basin and Range Province: nappe tectonics in an extending orogen. *Nature*, **291**, 645–648, https://doi.org/10.1038/291645a0

Whitney, D.L., Teyssier, C. and Vanderhaeghe, O. 2004. Gneiss domes and crustal flow. *Geological Society of America Special Papers*, **380**, 15–33, https://doi.org/10.1130/0-8137-2380-9.15

Whitney, D.L., Teyssier, C., Rey, P. and Buck, R.W. 2013. Continental and oceanic core complexes. *Geological Society of America Bulletin*, **125**, 273–298, https://doi.org/10.1130/B30754.1

Williams, I.S. 1997. U-Th-Pb Geochronology by Ion Microprobe. *In*: McKibben, M.A., Shanks, W.C. and Ridley, W.I. (eds) *Applications of Microanalytical Techniques to Understanding Mineralizing Processes, Reviews on Economic Geology*. Society of Economic Geologists, 1–35, https://doi.org/10.5382/Rev.07.01

Yin, A. 2004. Gneiss domes and gneiss dome systems. *Geological Society of America Special Papers*, **380**, 1–14, https://doi.org/10.1130/0-8137-2380-9.1

Zwart, H.J. 1979. The geology of the Central Pyrenees. *Leidse Geologische Mededelingen*, **50**, 1–74.